AIMS Materials Science, 3(3): 1054-1106.
DOI: 10.3934/matersci.2016.3.1054
Received: 29 June 2016
Accepted: 24 July 2016
Published: 29 July 2016

http://www.aimspress.com/journal/Materials

Review

Composite anodes for lithium-ion batteries: status and trends

Alain Mauger [1], Haiming Xie [2,*], and Christian M. Julien [3,*]

[1] Sorbonne Universités, Univ. UPMC, Paris-6, Institut de Minéralogie et Physique de la Matière Condensée (IMPMC), 4 place Jussieu, 75252 Paris, France
[2] Northeast Normal University, National & Local United Engineering, Laboratory for Power Batteries, 5268 Renmin Str., Changchun, P.R. China
[3] Sorbonne Universités, Univ. UPMC, Paris-6, Physico-Chimie des Electrolytes et Nanosystèmes Interfaciaux (PHENIX), UMR 8234, 4 place Jussieu, 75005 Paris, France

* **Correspondence**: E-mail: Christian.Julien@upmc.fr; xiehm136@nenu.edu.cn.

Abstract: Presently, the negative electrodes of lithium-ion batteries (LIBs) is constituted by carbon-based materials that exhibit a limited specific capacity 372 mAh g^{-1} associated with the cycle between C and LiC_6. Therefore, many efforts are currently made towards the technological development nanostructured materials in which the electrochemical processes occurs as intercalation, alloying or conversion reactions with a good accommodation of dilatation/contraction during cycling. In this review, attention is focused on advanced anode composite materials based on carbon, silicon, germanium, tin, titanium and conversion anode composite based on transition-metal oxides.

Keywords: composites; anode materials; conversion reaction; alloying; intercalation; Li-ion batteries

1. Introduction

Among all of the power sources, lithium ion batteries (LIBs) have become one of the most important and efficient devices for storage of electrical energy generated from renewable sources such as solar and wind energy, and they are currently used to solve the intermittence problem of these renewable energy sources for their integration in grid-scale stationary storage [1]. However, the LIBs that are commercialized today cannot yet satisfactorily meet the energy requirements for HEVs/EVs, and the increase of the energy density without sacrificing the safety is the subject of

intensive research. So far, the most popular material used as the anode of commercial Li-ion batteries is graphitic carbon. Its theoretical capacity, however, is only 372 mAh g^{-1}, while the total capacity of a Li-ion cell is expected to increase significantly with anode capacity up to 500 mAh g^{-1} approximately. For larger anode capacities, the total capacity reaches saturation because of the limitation imposed by the cathode [2]. There is thus a strong motivation to find an active anode material that would substitute carbon to reach a larger capacity. This is a difficult task, however, because the capacity is not the only pertinent parameter. One advantage of the carbon is the controlled formation of a stable solid-electrolyte interface (SEI) that is formed during the first cycles. Also, the volume change during the lithium insertion or delithiation must be controlled to avoid pulverization or simply breaking of the SEI, which would result in aging of the cell and loss of capacity upon cycling. In addition, the ionic and electronic conductivities should be as large as possible to obtain a large power density. Many materials synthesized under different shapes have been proposed, whether the lithium transport is due to intercalation, alloying, or conversion reactions. We have recently reviewed them in [3]. Figure 1 illustrates the potential vs. Li^0/Li^+ and the corresponding specific capacity of the next generation of active anode materials. The trend is the reduction of the size of the active particles to the nanometric range. The advantage is a shorter path for the Li^+ ions and the electrons in the particles, which allows a faster charge and discharge. Moreover, the effective surface area between the active particles and the electrolyte is enhanced, which reduces the internal resistance of the cell.

The reduction in size to the nano-range is also needed to accommodate the volume deformation and prevent the fracture during lithiation and delithiation. Indeed, excellent mechanical properties are also necessary for high-capacity anode materials the physical mechanisms such as volume deformation and fracture during lithiation and delithiation are currently the suject of intensive research. The conditions to avert fracture and debonding of hollow core-shell nanostructures in terms of the core radius, the shell thickness, and the state of charge have been determined by Zhao et al. [4], modeled in [5], and simulated by using a non-linear diffusion lithiation model [6]. Optimal conditions for the full use of inner hollow space were identified in terms of the critical ratio of shell thickness and inner size and the state of charge by Jiang et al. [7]. Fracture mechanics was used to determine the critical conditions to avert insertion-induced cracking [8]. A bridge between hardness and state of charge for electrodes in lithium-ion batteries by introducing electrochemistry-induced dislocations was proposed by Wang et al. [9]. For Si anodes, the critical sizes of fracture for different shapes of Si have been found to be 90 nm for nanoparticles, 70 nm for nanowires, and 33 nm for nanofilms, below which the silicon nanostructures remain undamaged upon lithiation [10]. The critical sizes of thin films and nanoparticles below which cracking would not occur has been investigated in [11]. The surface cracking of Si particles has been investigated through calculations in an elastic and perfectly plastic model [12]. The mechanical properties of Li-Sn alloys have been published by first-principle studies [13,14] and finite element modeling [15].

The reduction of the size of the particles to the nanometric range is not sufficient to ensure high capability and high power density; however, all the criteria in terms of ionic and electronic conductivity and stability upon cycling can hardly be met in any single material. That is why recent works proposed composites that mix active elements with complementary properties, like carbon for its high electronic conductivity, and silicon for its high energy density for instance, aiming to obtain

the best compromise between these different properties. Indeed, the only alternative to carbon anodes that encountered a success at the industrial scale is the composite Sn/Co/C commercialized by Sony in 2005 [16]. Since then, many other nanocomposites have been proposed as anode materials for next generation of Li-ion batteries. The aim of this section is to review them and report on the state-of-the-art in the investigation of composites as anodes for Li. Bs. Note that the reader is guided to the review [3] that contains 660 references for any work related to the synthesis and properties of the single components of the composites. Since then, however, progress has been made for the synthesis of composite nanofibers by electrospinning and centrifugal forcespinning (FS) for use as anodes in LIBs. They have been reviewed in [17]. Although electrospinning has been widely used as a synthesis process of electro-active nanofibers for constructing high performance materials for Li-ion batteries (see [18,19] for review). FS can produce fibers from melt and solutions without the need of applying an electric field during processing. Furthermore, the FS method has proven to be suitable for the mass production of nanofibers. To preserve a reasonable length to this section, we have chosen to omit any detail on the synthesis. This is a paradox, since the progress in the synthesis process of the nanocomposites is obviously the reason for the progress in their performance. However, the synthesis process is usually well described in the publications. Moreover, a significant progress has been reported on the synthesis and fabrication of composite materials for applications in LIBs [20] where the voltage limits of the anodes are discussed. The recent progress in enhancing the LIBs performance of TiO_2 with various synthetic strategies and architectures control has been reviewed in [21,22]. The properties of porous structures and their applications to negative electrodes for rechargeable lithium-ion batteries have been reviewed in [23]. An overview of several novel fabrication techniques of the electrodes for improving the electrochemical performance of silicon-based anode materials and their possible mechanisms are given in [24]. Various approaches to design materials in the form of 0, 1 and 2D nanostructures and their effect of size and morphology on their performance as anode materials in LIBs have been reviewed in [25].

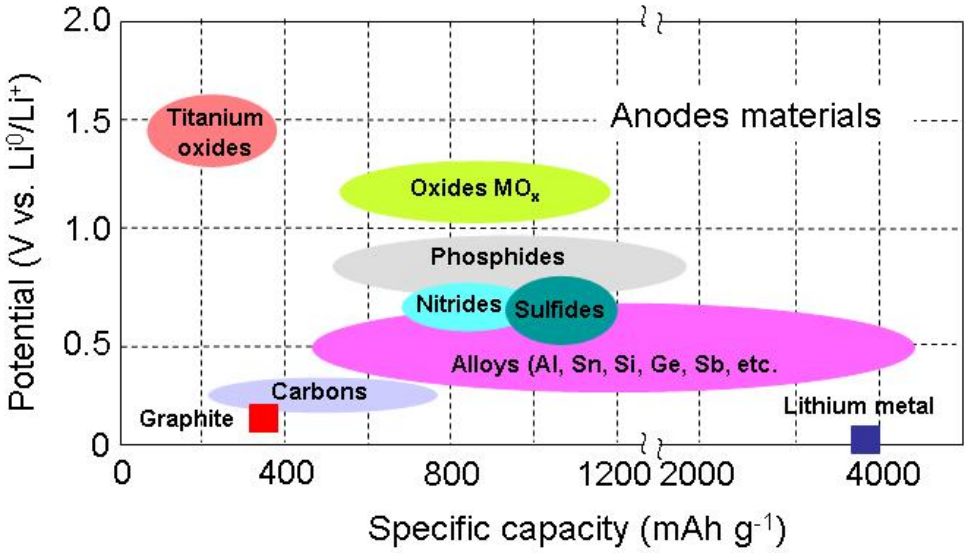

Figure 1. The potential vs. Li^0/Li^+ and the corresponding specific capacity of the next generation of active anode materials.

Taking these considerations into account, in this review, we focus attention on the electrochemical properties of the composites, although the best electrochemical properties obtained with the components are reported for the sake of comparison and discussion. The progress has been so fast that also made the choice to report on the works mainly published the last five years. We guide the reader to elder review papers on anode materials for prior works [26,27]. Finally, compared with $Li_4Ti_5O_{12}$, niobium based oxides have similar lithium ion insertion/extraction potential and have a similar good rate performance and promising to be new anode materials with high power performance. Only $Li_4Ti_5O_{12}$ as an anode component has been reviewed here, while Nb-based oxides as anodes have been reviewed in [28].

2. Carbon-based Anodes

2.1. Carbon Nanotube Composite Anodes

Carbon nanotubes (CNTs) have good thermal and mechanical properties, together with a good conductivity. They are thus candidates for use as anodes in Li-ion batteries. However, the performance will depend strongly on the quality of the SEI, which is a function of the quality of the surface. This is actually a drawback of the decrease of the size of the particles to the nano-range: as the effective surface in contact with the electrolyte is larger, the SEI effects become more critical. This has been the motivation for coating the nanotubes or the graphene sheets to protect them. In particular, The deposition of a 10 nm-thick layer of Al_2O_3 on the multi-wall carbon nanotubes (MWCNTs) by atomic layer deposition delivered a reversible capacity of 1100 mAh g^{-1} in 50 cycles at the current rate of 372 mA g^{-1} [29]. This is the best result obtained with MWCNTs so far. The effect of Al_2O_3 is the blocking of the electron tunneling to the adsorbed ethylene carbonate (EC) molecules of the electrolyte, thus decreasing its decomposition [30]. Therefore, the Al_2O_3 coat acts as an artificial SEI, which is beneficial for the performance of the MWCNTs. For comparison, the capacity delivered by commercial MWCNTs is close to 250 mAh g^{-1}, raising to 400 mAh g^{-1}after purification. Some good results have also been obtained with composites of carbon nanotubes and other active nanostructured materials [31]. For instance, SnSb particles finely encrust within the mesh-like CNT framework, which consisted of well dispersed CNTs, delivered a reversible capacity of 860 mAh g^{-1} during the 40th cycle at a current density of 160 mA g^{-1} [32]. The uniform Fe_3O_4 coating of aligned carbon nanotubes by magneton scattering used as an anode delivered 800 mAh g^{-1} over 100 cycles [33]. Composite electrodes consisting in Fe_3O_4 nanorods and 5 wt% single wall carbon nanotubes as a conductive net delivered over 1000 mAh g^{-1} after 50 cycles at 1C-rate, 800 mAh g^{-1} at 5C and still 600 mAh g^{-1} at 10C [34]. One can also cite MoS_2/MWCNT composite electrode that delivered 1030 mAh g^{-1} after 60 cycles [35]. However, carbon nanotubes did not find a market to commercial use. Their growth rate is still too low, they are expensive and it is difficult to prepare them free of impurity. Moreover, the atomic layer deposition used in [29] is a remarkable process to deposit well-controlled surface layers, but it is also expensive. In addition, the CNTs suffer from a tendency of embrittlement upon cycling because the morphology of the nanotubes does not allow the expansion of the graphene sheets in the c-axis or radial direction as in graphite.

2.2. Graphene Composite Anodes

Due to the elasticity, strong mechanical resistance, good electronic conductivity, large surface area, graphene is an attractive anode material. In addition, the theoretical capacity is 780 mAh g^{-1} if Li can be absorbed on both sides up to the chemical formula Li_2C_6, and 1116 mAh g^{-1} if Li can be trapped at the benzene rings up to LiC_2. The best performance has been obtained with N- and S-doped hierarchically porous graphene electrode that showed a high power density (116 kW kg^{-1}) and high energy density (322 Wh kg^{-1}) at current density 80 A g^{-1} (only 10 s to full charge) [36]. Graphene can thus be used for its intrinsic properties. Moreover, it is also used in composites with another electroactive anode material for two reasons. First, the grafted nanoparticles prevent the graphene sheets from re-stacking that is a major cause of capacity fading upon cycling. Second, the graphene is an elastic support that helps the nanoparticles to accommodate their volume change upon lithium insertion or delithiation without breaking or pulverization, another source of aging. Third, such electrodes may not require the need for binders, which reduces the cost of fabrication and maximizes the content in active materials and thus the capacity. Therefore, many works have been published on graphene-based composite anodes, which have been reviewed in [37]. We shall report and discuss the state-of-the-art of such composite anodes in the following sections devoted to the metals and metal oxide counterparts. The important irreversible capacity during the first cycle is due the formation of the SEI, and also in some cases due to irreversible reaction in the first cycle. Therefore, we always report the stabilized reversible capacity after several cycles, which is the capacity of interest for practical use of a secondary battery.

The incorporation of graphitic carbon nitride into graphene results in a g-C_3N_4/graphene (CN-G) hybrid that exhibits improved Li^+ storage capacity and rate capability with respect to the pristine g-C_3N_4 and graphene [38].

3. Silicon-based Composites

With a huge theoretical capacity (4200 mAh g^{-1}), Si is a cheap and abundant material that has attracted a huge interest as a prospective replacement of graphite anode, inasmuch as the material processing is well known owing to its use in electronics. However, the huge volume change ~400% between Si and $Li_{22}Si_5$ causes cracking and pulverisation, resulting in poor cycling that hinders its commercial use. Nevertheless some solutions have been found to overcome this problem, which in any case require the use of nanosized Si under different shapes.

3.1. Si Films

It is possible to obtain long cycling life up to 3000 cycles with Si films prepared by physical vapor deposition [39,40] and magnetron sputtering [41]. A 50 nm-thick film of n-doped Si film with phosphor to improve the electronic conductivity, deposited on to a 30-μm thick Ni foil, maintained a capacity of 3000 mAh g^{-1} at rate 12C over 1000 cycles. Even at heavy load at 30C rate, the capacity was still 2000 mAh g^{-1} after 3000 cycles [42].

In an attempt to improve these performances that are already remarkable, attempts have been

made to synthesize multi-layer composites. Good results were already obtained more than 10 years ago with Fe-Si multi-layer composite prepared by alternate deposition using an electron-beam evaporation method. The layer thickness was 9.5 nm and 7.5 nm for the Si (active) and the Fe (inactive) films, respectively [43]. After annealing a Fe-Si alloy is formed at the Si/Fe interface, which acts as a buffer layer for alloy reaction of Si with Li [44]. This material used as an anode delivered a specific capacity 3000 mAh g^{-1} over 300 tested cycles at charge and discharge current 30 A cm^{-2} between 0 and 1.2 V at 30 °C. More recently, another multilayer made of 50 nm-thick Si films and a soft elastomeric substrate (poly(dimethylsiloxane)) acting as a buffer layer exhibited a discharge capacity of 3498 mAh g^{-1} at C/4 current rate with 84.6% capacity retention over 500 charge/discharge cycles [45].

Coating with a metal oxide was chosen to protect direct contact between the Si nanostructure and the electrolyte. The best results have been obtained with Al_2O_3 coating. Upon the first lithiation, this oxide transforms into Al-Li-O glass [46]. This glass is an electrical insulator, but a good ionic conductor, which are the attributes of a good SEI substitute. Of course, in that case, the thickness of the coating layer must be small in order to minimize the increase of electrical resistivity induced by the coating. In practice, the thickness of the Al_2O_3 obtained by atomic layer deposition (ALD) is smaller than 10 nm, and has been tested successfully on Si thin films [47,48]. Note that it is difficult to make a quantitative comparison between the different works on Si thin films, because the performance depends dramatically of the deposition rate, temperature of the deposition, film thickness, annealing treatment.

3.2. Nanostructured Si Nanowires and Nanotubes

The shape of the Si material also matters. The nanotubes and nanowires are less prone to cracking and pulverization than nanoparticles upon cycling. They can also be connected electrically to the current collector more easily than nanoparticles. That is why many efforts have been made to prepare them and test them (see the review in [23]). In particular, porous B-doped Si nanowires recorded 2000 cycles at 18 A g^{-1} current density, with a remaining capacity still larger than 1000 mAh g^{-1} [49]. The mass loading, however, was small (0.3 mg cm^{-2}). This is one major problem with these Si anodes: high rate capability is obtained only at low mass loading. Figure 2 shows the HRTEM images of silicon nanowires before (a) and after (b) lithiation (10th cycle at current rate of 0.4 A g^{-1}) [49].

Even if the porous structure and shape can help in the prevention of cracking, it does not solve the problem of the SEI. In particular, once the silicon has been lithiated, the delitiation induces a contraction that can break the SEI layer, which results in a new Si area in contact with the electrolyte, and more SEI is thus formed. The resulting increase of the thickness of the SEI layer means more consumption of the electrolyte, an increase of the electrical and ionic resistance, in short aging of the cell. The strategy to overcome this problem is to coat the silicon with a protective layer. Si nanowires were coated with carbon to build a mesoporous Si@carbon core-shell nanowires with a diameter of <6.5 nm [50]. They were prepared by a SBA-15 hard template. The nanotubes were formed by filling the void space of the template to form an inverse porous structure. This is one example among many others that illustrates the efficiency of inverse opal nanoarchitecture as lithium ion anode materials,

to which a recent review has been dedicated [51]. In [50], butyl terminators in the Si-C_4H_9 precursor formed a capping that protected Si from reacting with SiO_2 during annealing and converted to carbon shell layers later in the annealing process. These carbon-coated nanowires retained a capacity at 2738 mAh g^{-1} after 80 cycles. The efficiency of the carbon shell depends on its thickness. 10 nm-thick carbon coating on Si nanowires of 90 nm in diameter increases the initial capacity to 3700 mAh g^{-1} (compared to 3125 mAh g^{-1} before coating) and the capacity retention is raised to 86% after 15 cycles [52]. Unfortunately no test has been reported after few hundreds cycles. Si nanowires were also embedded in a network of carbon nanotubes.

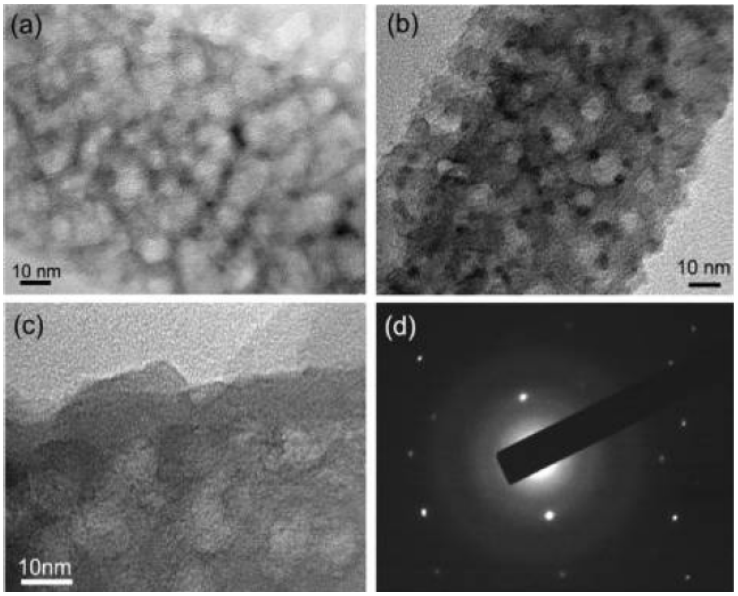

Figure 2. HRTEM images of B-doped silicon nanowires before (a) and after (b) lithiation (10th cycle at current rate of 0.4 A g^{-1}). (c) Enlarged HRTEM showing the amorphous Si structure. (d) SAED pattern showing the crystalline Si in black spots in (b) (from Ref. [49]).

Replacing the 10 nm-thick carbon coating on the Si nanowires with a Cu coat of same thickness improves the coulombic efficiency in the first cycle to 90% and the capacity retention to 86% after 15 cycles. This effect can be attributed to the fact that Cu is a better electrical conductor than the carbon coat. For the same reason, the Cu-coating of Si thin films also improved the performance [53] The cycling properties of silicon nanowires has also been improved by coating them with a conductive polymer like (3,4-ethylenedioxythiophene) PEDOT [54].

Cu can be replaced by another metal coating. However, Al coating has a different effect: it does not improve the coulombic efficiency of the first cycle but it improves the capacity retention of nanowires [55], mainly because it improves the mechanical structure of the anode [56,57]. Similar results were obtained by coating the Si nanowires with a 100 nm-thick Ag/PEDOT improving the capacity retention to 80% after 100 cycles [54].

The coating with a metal was intended to increase the electrical conductivity which is beneficial to the electrochemical properties because Si is a semiconductor. On another hand, Si nanowires have

also been coated with Al_2O_3, to avoid direct contact between Si and the electrolyte, like the Si thin films previously mentioned. The Al_2O_3 coating of Si nanowires increased the anode lifetime up to 1280 cycles when the capacity is limited to 1200 mAh g^{-1} and exhibited a discharge capacity of 1 Ah g^{-1} at 12 C current rate after 6000 electrochemical cycles [58].

In a different approach, a stiff shell can reduce the mechanical stress of the Si nanostructures and clamp them. The Si nanotubes with a clamping SiO_x layer exhibited a discharge capacity of 1000 mAh g^{-1} at 12C current rate after 6000 electrochemical cycles [59]. The coat of Si nanotubes by rigid carbon also proved to be successful to control their growth [59]. In the same spirit, Si nanotubes were coated with Ge [60,61], SnO_2 [62] and TiO_2 [61]. Nevertheless, these coatings had little effect on the initial coulombic efficiency, except Ge coating. The reason is that these coating materials are almost inactive in the potential window 0.02–1.2 V. On another hand, they all improved significantly the life of the battery, so that they efficiently avoided the direct contact between Si and the electrolyte.

More complex structures were elaborated such as aligned carbon nanotubes uniformly coated with Si and a thin layer of carbon on top of it [63]. Used as an anode, this architecture demonstrated very good stability up to the 250 cycles that were tested and high capacity of 4200 mAh g^{-1}. Still this performance is obtained at low C-rate. Good results have been obtained at high C-rate with amorphous carbon nanorods with an intermediate layer of aluminum that is finally capped by a silicon nanoscoop on the very top [64]. This structure maintained a capacity of 412 mAh g^{-1} over 100 cycles at 40C rate, corresponding to a current density 51.2 A g^{-1}. The thin layer of carbon at the top of Si was found essential to obtain the good performance in [63], which suggests that Si particles cracked and avoided the exposure to fresh Si to the electrolyte only because the carbon could protect the Si part from any direct contact with the electrolyte. On the other hand, the very good results even at high C-rate in [64] proves that the aluminum intermediate layer enables the gradual transition of strain from carbon to silicon so that the integrity of the Si layer is kept during cycling.

3.3. Si Nanoparticles

To facilitate this contact, and keep it along cycling, Si nanoparticles can be dispersed in a more conductive medium, usually carbon, to form a C-Si composite. The results, however, were not satisfactory unless the amount of carbon is the order of 50%, i.e. about one order of magnitude larger than required for any application. One exception is the work of Cho et al. [65] who fabricated carbon-coated porous Si particles (pore size 40 nm). The carbon coating accounted for 12 wt% of carbon and such particles delivered 2800 mAh g^{-1} over 100 cycles at 1C rate.

Recent progress has been made by coating Si nanoparticles with 2–10 layers of graphene, anchored directly to the Si particle surface at their ends, and lying parallel to the Si surface. These layers accommodate the volume expansion of silicon via a sliding process between adjacent graphene layers. When paired with a commercial lithium cobalt oxide cathode, the silicon carbide-free graphene coating allows the full cell to reach volumetric energy densities of 972 and 700 Wh L^{-1} at first and 200th cycle [66].

Another strategy to accommodate the huge change of volume during the alloying-de-alloying reaction was to elaborate composite materials with Si nanoparticles embedded in a hollow structure

such as a hollow carbon nanotube [67]. Due to the hollow space inside the nanotube, the carbon tube is not damaged during the volumetric change during cycling. The corresponding electrode delivered an initial capacity of 969 mAh g^{-1}. Taking the carbon mass into account, it corresponds to a capacity of 2061 mAh g^{-1} for the silicon itself. The capacity retention was 90% after 200 cycles at current density 1 A g^{-1}. In the same way a Si@void@C electrode was built, with the property that the Si nanoparticle expanded without breaking the carbon coating in which it is embedded, owing to the void space [68]. The capacity was 2833 mAh g^{-1} for the first cycle at C/10 current rate and stabilized at ≈1500 mAh g^{-1} for later cycles at 1C current rate. A hierarchical pomegranate structured Si-C composite electrode delivered 2350 mAh g^{-1} at C/20 current rate and over 1160 mAh g^{-1} after 1000 cycles at a current rate of C/2 [69].

Due to the very good electrical conductivity and mechanical properties, Si nanoparticles-graphene composites have been investigated, with significant progress in the electrochemical properties through the years. In 2010, the corresponding electrodes delivered 1168 mAh g^{-1} and an average coulombic efficiency of 93% up to 30 cycles [70], 708 mAh g^{-1} at a current density of 50 mA g^{-1} after 100 cycles [71], 1350 mAh g^{-1} at a current density of 1 A g^{-1} after 300 cycles [72]. Hierarchical three-dimensional carbon-coated mesoporous Si nanospheres@graphene foam delivered specific capacities of 1104 mAh g^{-1} and 969 mAh g^{-1} at 500 mA g^{-1} and 1 A g^{-1} after 200 cycles, respectively. Even at a current rate of 10 A g^{-1}, the electrode still achieved a capacity of 659 mAh g^{-1} after 200 cycles [73]. In 2011, Zhao et al. reported 2600 mAh g^{-1} at 8 A g^{-1} current rate after 150 cycles [74]. In 2014, the same group reported 1120 and 700 mAh g^{-1} after 1000 cycles at a current density of 0.5 and 2.1 A g^{-1}, respectively, due to sheathed Si particles in graphene sheets, leading to a buffering effect from pulverization and electrical isolation of the active materials [75]. In this later case, the performance was attributed to enveloping carbon/SiOx sheathed Si particles in graphene sheets.

The progress made in the performance of Si-based anodes is remarkable, but still Si is barely competitive with commercial carbon-based anodes that store a charge of 4 mAh cm^{-2}, owing to their 50-μm thick film on the current collector. Such a thickness is not possible with Si-based anodes, because of the huge change of volume during cycling. Assuming a Si capacity of 3800 mAh g^{-1}, an areal mass of at least 1 mg cm^{-2} of Si is required to be competitive. If the Si is under the form of nanowires, their thickness should be 300 nm to fulfill this condition, which would limit the rate to 3C [76]. Si films are closer to the performance required to be competitive, since they are now able to deliver 1.8 mAh cm^{-2}. Note, however, that the Si films are usually prepared by physical vapor deposition of magnetron sputtering that is not cheap synthesis process. With nanotubes, we also meet the difficulty to combine high charge and power. The overall thickness of the electrode and the synthesis process are a limiting factor. Nevertheless, two scalable methods to produce Si-based nanotubes have been proposed recently [63,77], opening the route to their mass production in the near future.

4. Germanium

The theoretical capacity of Ge is 1624 mAh g^{-1}. At contrast with Si, Ge is very expensive, which prevents so far its commercial use, but it also has important advantages over Si: a better

electronic and ionic conductivity, and a huge theoretical capacity since it can be lithiated to Li_5Ge_4 [78]. In addition, contrary to the case of Si, the dilatation/contraction of the lattice upon lithiation/delithiation is isotropic so that the particles avoid cracking even at high C-rate and big particles 620 nm in size [79,80]. As a result of these properties, the rate capability of Ge is quite remarkable [81]. Germanium-graphene composites retained a capacity of 675 mAh g^{-1} after 400 cycles at current density to 400 mA g^{-1}; Ge-graphene composite anode for high-energy lithium batteries with long cycle life [82]. Recently, germanium (Ge) nanoparticles anchored on reduced graphene oxide intertwined with carbon nanotubes (CNT) delivered a capacity of 863.8 mAh g^{-1} at a current density of 100 mA g^{-1} after 100 cycles and good rate performances of 1181.7, 1073.8, 1005.2, 872.0, 767.6, and 644.8 mAh g^{-1} at current densities of 100, 200, 400, 800, 1600, and 3200 mA g^{-1}, respectively [83]. Germanium 60 nm-thick nanoparticles (Ge-NPs) were synthesized through a one-step chemical vapor deposition process and were included in a hybrid free-standing SWCNT electrode [84]. As an anode, this composite delivered a capacity of 983 mAh g^{-1} versus Li^0/Li^+ up to 3 V at low current density 50 mA g^{-1}, and 780 mAh g^{-1} up to 1.5 V. The reversible capacity is maintained at 750 mAh g^{-1} in cycles up to 1.5 V at current density of 200 mA g^{-1}.

So far, the results reported on the anodes have been measured on half-cells with lithium counter-electrodes. Since the major advantage of Ge with respect to the other active anode materials (except $Li_4Ti_5O_{12}$ that will be discussed later) is the high rate capability. It is of interest to test a full cell where the active element of the positive electrode is also known for its outstanding rate capability, i.e. carbon-coated $LiFePO_4$. This has been done in [84] with the anode mentioned above. This full cell demonstrated a good capacity retention almost independent of the C-rate up to 1C.

Other improvements on Ge anodes have been made in 2014–2015, which have not been reported here, as a recent review on Si anodes has made focus on these two years, and we just guide the reader to this work. As an example, Figure 3 presents the discharge-charge curves at a rate of 0.1 A g^{-1} (a) and Nyquist plots (b) of pure Ge, Ge-RGO and Ge-RGO-CNT nano-composite anodes [85].

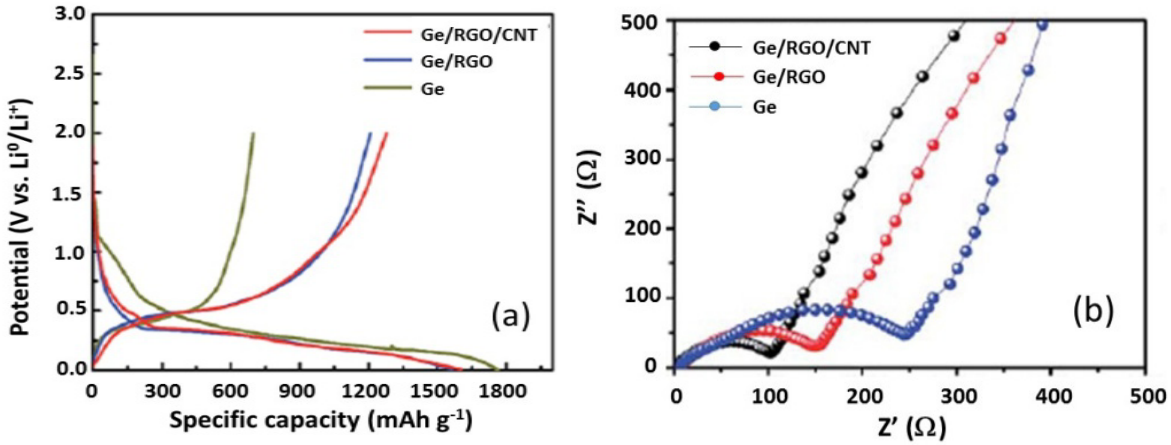

Figure 3. Discharge-charge curves at a rate of 0.1 A g^{-1} (a) and Nyquist plots (b) of pure Ge, Ge-RGO and Ge-RGO-CNT nano-composite anodes (from Ref. [85]).

5. Tin-based Composites

With a maximum of 4.4 Li per Sn, the theoretical capacity of Sn is 993 mAh g^{-1}, but the huge change of volume (260 % up to full lithiation) looks prohibitive. At least, if makes mandatory the preparation of composite structures to maintain electrical contact and separate, the Sn nano-structured elements so that they can accommodate this huge variations of volume. Without any surprise, the most popular composite element tested for this purpose was carbon, inasmuch as its reactivity with Sn is small (see [86] for a review dating from 2011). A composite of 3.5 nm Sn nanoparticles dispersed in nitrogen-doped carbon retained a specific capacity of 660 mAh·g^{-1} at the 200th cycle and a 630 mAh·g^{-1} capacity at 400th cycle at 0.2 A g^{-1} current density [87]. This illustrates how efficient is the decrease of the size of the active particles to the nano-size to accommodate their volume change during cycling and thus enhance the cycling life of the batteries. Among Sn/C composite, Sn particles encapsulated with carbon nanofibers was promising, as it delivered a capacity of 800 mAh g^{-1} after 200 cycles [88]. This is a major improvement with respect to a Sn@C core-shell composite that showed a capacity retention of 400 mAh g^{-1} after 50 cycles at the current density of 100 mA g^{-1} [89]. This illustrates the advantage of the nanofiber morphology of the carbon additive to enhance the electrochemical performance of anodes. The only Sn-graphene composite that has been reported to our knowledge [90] delivered a reversible capacity over 100 cycles at current density 100 mA g^{-1}. Recently, a new scalable technique, forcespinning (FS) was used to produce binder-free porous Sn/C composite nanofibers [91]. These highly flexible Sn/C composite nanofibers were directly used as binder-free anodes for lithium-ion batteries. The produced Sn/C composite nano fibers showed an improved discharge capacity of about 724 mAh g^{-1} at a current density of 100 mA g^{-1} for over 50 cycles compared to most nanofiber electrodes prepared by electrospinning and centrifugal spinning.

Amorphous nano-composites made of an active (Sn) and inactive (transition metal M) along with some graphitic metal were also proposed with *M* = Mn [92], Fe [93,94,95], Co [96,97,98], Ni [99], Cu [100]. The best results were obtained with Sn-Co-C, because cobalt does not react with carbon and does not form carbides [101]. $Sn_{0.31}Co_{28}C_{0.41}$ delivered a stable capacity of 500 mAh g^{-1} up to C/4 rate [102], which means 350 mAh g^{-1} if we take into account the mass of inactive carbon. This is comparable to the gravimetric capacity of graphite, but the volumetric capacity is enhanced by 600% due to the Sn/Co density of 14.3 g cm^{-3}. Sony has commercialized a 18650 Li-ion battery with a Sn-Co-C anode and $LiCoO_2$ cathode, named Nexelion, the capacity of which is 3.5 Ah [16,103]. A Cu_6Sn_5-Cu_3Sn-carbon nanotubes composite anode showed a good cycling performance, with a capacity 513 mAh g^{-1} after 100 cycles at 1C rate, and a good rate capability, with a capacity of 411 mAh g^{-1} at 16C rate [104]. More recently, nanosized Sn particles embedded in electrically conducting porous multichannel carbon 350 mAh g^{-1} after 600 cycles, most of them performed at 2C rate [105].

A composite made of amorphous nanoporous SnO (nanopores distributed randomly on the surface with a diameter ranging from about 1 nm to over 20 nm) and carbon nanotubes (CNTs) was synthesized by electrodeposition and anodic oxidation methods. The BET surface area of the composite was 53.4 m^2 g^{-1}, and the total pore volume is 0.151 cm^3 g^{-1} [106]. This composite as an anode delivered a reversible capacity of 1608 mAh g^{-1} at a current density of 100 mA g^{-1},

maintaining at 732 mAh g^{-1} at the 50th cycle.

Attention has been more focused on tin oxide SnO_2. It reacts with Li according to the two steps:

$$SnO_2 + 4\ Li^+ + 4\ e^- \rightarrow Sn + 2\ Li_2S, \quad (1)$$

$$Sn + x\ Li^+ + x\ e^- \rightarrow Li_xSn\ (0 \leq x \leq 4.4) \quad (2)$$

The first reaction is irreversible and results in an irreversible loss of reversible capacity of 711 mAh g^{-1}. Nevertheless, Li_2O has a major advantage: it acts as a buffer and helps to mitigate the volume changes associated to the second reversible reaction. This is not sufficient, however to solve entirely the problem, and in this case too, composites have been made to improve the cycle ability.

5.1. Thin Films

In the form of thin films, good results were obtained with the combination Sn-CoO [107] and Sn-MnO [108]. In the case of Sn-cobalt oxide, the reversible capacity of 734 mAh g^{-1} increased after 50 cycles to 845 mAh g^{-1}. This increase of capacity upon cycling is often met with tin-based anodes, and is due to the better lithium accessibility in the composite during the cycling.

5.2. Coated SnO_2

Coating SnO_2 was another option and the results improved constantly the last decade. 6–10 nm-thick SnO_2 nanoparticles coated with carbon forming a composite with 8 wt% carbon showed a capacity of 631 mAh g^{-1} after 100 cycles at current 400 mA g^{-1} [109]. More recently, carbon-coated SiO_2 nanospheres synthesized via a one-spot hydrothermal method end subsequent carbonization delivered 1215 mAh g^{-1} after 200 cycles at current density of 100 mA g^{-1}. The reversible capacity is maintained at 520 mAh g^{-1} at current density 1600 mA g^{-1} [110]. A carbon-coated SnO_2-NiO multicomposite delivered 529 mAh g^{-1} and 265 mAh g^{-1} after 500 cycles at current density 800 and 1600 mA g^{-1}, respectively [111]. These results show that it is now possible to obtain nano-structured SnO_2 based composites that maintain the integrity of the structure upon cycling, even at high rate. A promising result was obtained by coating SnO_2 particles not with carbon, but with HfO_2 [112]. This anode was able to deliver a capacity of 853 mAh g^{-1} after 100 cycles at a low current density (150 mA g^{-1}). In this case, HfO_2 acts as a passivation layer. SnO_2 was also uniformly decorated with polypyrrole (Ppy) nanowires to obtain an anode that delivered 690 mAh g^{-1} with 90% capacity retention up to 80 cycles [113].

Hollow geometry proved very efficient, since the voids give some place to maintain the structural stability during the volume changes experienced during cycling. In particular, SnO_2 hollow nanosphere coated with carbon (carbon content 32 wt%) delivered a stable capacity of 460 mAh g^{-1} and 210 mAh g^{-1} over 100 cycles at 0.8C and 4.8C, respectively, with 1C = 625 mA g^{-1} [114]. SnO_2 nanoparticles have also been deposited on the skeleton of inverse opal carbon monoliths [115]. There, the SnO_2 nanoparticles are confined within the mesoporous voids preventing the particles from disconnecting from the carbon. More recently, porous SnO_2 microboxes with a high uniformity and well-defined non-spherical hollow structure delivered 550 mAh g^{-1} after 150 cycles at current density 200 mAh g^{-1} [116].

5.3. SnO_2-Carbon Nanotubes

The composites obtained under the form of nanotubes showed good electrochemical properties, but at low C-rates only. A uniform layer of SnO_2 nanocrystals (crystal size 5 nm) on a multiwalled carbon nanotube delivered a stabilized capacity of 400 mAh g^{-1} over 100 cycles at current density of 100 mA g^{-1} [117]. More recently, better results were reported for such a nano-composite, which delivered 500 mAh g^{-1} for up to 300 cycles, owing to a novel ethylene glycol-mediated solvothermal-polyol route for synthesis [118]. The capacity of a SnO_2/multiwalled carbon tube core/shell structure remained at 720 mAh g^{-1} over 30 cycles at current density 0.2 mA cm^{-2} ,and the capacity fading was 0.8% per cycle [119]. A capacity of 540 mAh g^{-1} almost stable over 200 cycles at 0.5C rate was reported for porous SnO_2 nanotubes with coaxially grown carbon nanotubes overlayers [120].

Sandwich-like CNT@SnO_2/SnO/Sn anodes were prepared by using composite electrodeposition and anodic oxidation on three-dimensional (3D) Ni foam [121]. The poor coulombic efficiency from the first cycle to 10 cycles was attributed to the active mechanism of interface layers. But for the next cycles, the coulombic efficiency raised to 99% and the anode delivered a capacity of 394 mAh g^{-1} at the 50th cycle at a current density of 100 mA g^{-1}. The result suggests that the peculiar architecture of CNT encapsulated into SnO_x with 3D frame space can alleviate the huge volume variation of SnO_x.

5.4. SnO_2-Graphene Composites

The extensive study of SnO_2-graphite composites started in 2010–2011 [122–130]. Typically, the reversible capacity was maintained in the range 500–650 mAh g^{-1} for 50 cycles. However, a storage capacity of 775 mAh g^{-1} was reported by Zhao et al. [123]. Better results were reported more recently. A composite made of SnO_2 and graphene nanoribbons delivered a reversible capacity of 1130 mAh g^{-1}, maintained at 825 mAh g^{-1} after 50 cycles at current density of 100 mA g^{-1} [131]. Moreover the reversible capacity was 580 mAh g^{-1} at higher current density of 2 A g^{-1}. The high capacity of 1130 mAh g^{-1}, which is larger than the theoretical prediction for SnO_2, was attributed to the enhancement of the lithium storage by the graphene nanoribbons resulting from edge effects. The rate capability gives evidence of the ability of the graphene to buffer the volume change of the SnO_2 particles. An important improvement was obtained by using a hydrazine monohydrate vapor reduction method to bind 4–5 nm-thick SnO_2 nanocrystals in graphene sheets by Sn-N bonding [132]. Good capacity retention was obtained at 1074 and 417 mAh g^{-1} for current densities 0.5 and 20 A g^{-1}, respectively. The Sn-N bonding was confirmed by the analysis of the L3-edge peak intensity. This bonding that anchored the SnO_2 nanoparticles on the graphene sheets, then avoiding the agglomeration of the particles plus the small size of the particles, plus the high flexibility of the graphene explain this remarkable performance during long-term cycling tested over 500 cycles. Recently, non-doped SnO_2-reduced graphene oxide (RGO) composite as an anode delivered 1010 mAh g^{-1} per mass of the electrode at 0.05 A g^{-1} with a good capacity retention (470 mAh g^{-1}) even at 2 A g^{-1} (<2C) [133]. SnO_2/RGO nanocomposite showed a capacity retention of 500 mAh·g^{-1} after 50 cycles at 250 mAh g^{-1} [134]. F-doping of SnO_2 was also realized, improving significant improvement of the electrochemical properties of the SnO_2 nanocrystals-reduced graphene oxide

composite as shown in Figure 4 [135]. The chemical diffusion coefficients were calculated from the Z' vs. $\omega^{-1/2}$ plots as ~10^{-16} cm^2 s^{-1} for F-SnO_2@RGO and ~4 × 10^{-17} cm^2 s^{-1} for SnO_2@RGO. The composite delivered a reversible capacity of 1277 mAh g^{-1} after 100 cycles at current density 0.1 A g^{-1}. This capacity retention was at least partly attributed to the corrosion resistant properties of F-doping. The higher rate capability (634 mAh g^{-1} after 10 cycles at current density 5 A g^{-1}) was due to the reduced resistance induced by the F-doping that protects the electrode surface from the hydrolysis or decomposition of the $LiPF_6$ salt. SnO_2/graphene composite with superior cycle performance and high reversible capacity was prepared by a one-step microwave-hydrothermal method [136]. The capacity remains 1359 and 1005 mAh g^{-1} after 100 cycles at current densities of 100 and 700 mA g^{-1}, respectively. Even at current density of 1 A g^{-1}, the discharge specific capacity remained 1057 and 677 mAh g^{-1} after 420 and 1000 cycles, respectively. Finally, by providing an in-depth discussion of SnO_2/graphene nanocomposites, Deng et al. demonstrated that the electrochemical performances of SnO_2/graphene nanocomposites could be significantly enhanced by rational modifications of morphology and crystal structures, chemical compositions and surface features [137].

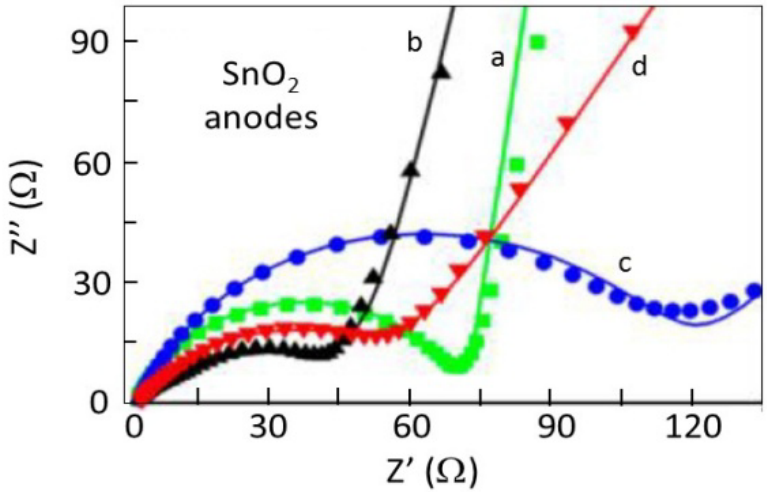

Figure 4. Nyquist plots of F-SnO_2@RGO (a,b) and SnO_2@RGO (c,d) electrodes measured at a fully charge state before (a,c) and after (b,d) charge/discharge. Chemical diffusion coefficients calculated from the Z' vs. $\omega^{-1/2}$ plots are ~10^{-16} cm^2 s^{-1} for F-SnO_2@RGO and ~4 × 10^{-17} cm^2 s^{-1} for SnO_2@RGO (from Ref. [135]).

Composites involving an additional element have also been elaborated. A core-shell structured Fe_2O_3-SnO_2 uniformly dispersed between layered graphene sheets delivered 1015 mAh g^{-1} after 200 cycles [138]. SnO_2 hollow spheres embedded in graphene sheets and enveloped by poly(3,4-ethylenedioxythiophene) (PEDOT) delivered 608 mAh g^{-1} after 150 cycles at current density of 100 mA g^{-1} , which amounts to 1248 mAh g^{-1} when only the mass of SnO_2 is considered [139].

These results and the progress that has been made in the last 6 years show that SnO_2-based composites are prospective anodes for Li-ion batteries. The main difficulty at this point is to switch

from the laboratory to the industrial scale, since the synthesis of these nanostructured composites is long and expensive. Scaling-up their preparation for commercial use at a reasonable price is the main challenge that needs to be solved for this material as many others to make possible the replacement of graphite by such composites. SnS_2 composites are reviewed in a forthcoming section devoted to sulfides.

6. Titanium Oxide-based Composites

6.1. TiO_2

TiO_2 is low cost and safe. Its theoretical capacity is 335 mAh g^{-1}, according to the reaction:

$$Ti^{4+}O^2 + x\ Li^+ + x\ e^- \leftrightarrow Li_x(Ti^{3+}_x Ti^{4+}_{1-x})O_2\ (x \leq 1) \quad (3)$$

This capacity is rather small with respect to other metal oxides reviewed here, but TiO_2 has an advantage over them: its dilatation upon lithium incorporation is smaller (except the "zero-strain" titanate that will be reviewed hereunder, but titanate has an even smaller capacity). That is why TiO_2 has been extensively studied as an anode material for Li-ion batteries.

Good results have been already obtained for TiO_2 without the need of another composite element. 3- and 4-shelled TiO_2 hollow microspheres capacity, up to 237 mAh g^{-1} with minimal irreversible capacity after 100 cycles is achieved at a current rate of 1C (167.5 mA g^{-1}), and a capacity of 119 mAh g^{-1} is achieved at a current rate of 10C even after 1200 cycles [140]. Mesoporous TiO_2 microspheres assembled from TiO_2 nanoparticles with specific surface areas as high as 150 m^2 g^{-1} delivered a high reversible capacity of <120.1 mAh g^{-1} when the current rate was increased from 0.2C to 5C after 50 charge-discharge cycles. Even at 10C, the capacity was still satisfactory (<100 mAh g^{-1}), with excellent reversibility [141]. However, better results can be obtained only in composites.

Like in the case of any metal oxide, composites have been formed with carbon under different structures. The carbon coating on TiO_2 enhances the electronic conductivity and provides space for suppressing the large volume expansion during cycling, which improved the electrochemical performance [142]. Carbon nanotubes were conjugated with all the active anode elements because of their high mechanical properties, low gravity, and high surface area; in addition, in the present case, they efficiently provide electrons to the nanostructure through the formation of Ti-C bonds, which helps in the insertion of lithium [143]. Indeed, the anatase TiO_2-C nanotubes in this work demonstrated a superior Li storage capacity of 320 (±68) mAh g^{-1}.

Many works have been made to prepare composites with graphene. It took some time to obtain good results, because the strong π-interaction of graphene was an obstacle to the homogeneous dispersion of TiO_2. However, the results obtained the last years are outstanding. A three-dimensional (3D) foam architecture of TiO_2 nanoparticles embedded in N-doped (high-level nitrogen content of 7.34%) graphene networks delivered a capacity of 165 mAh g^{-1} after 200 cycles at 1C rate, 143 mAh g^{-1} after 200 cycles at 5C rate [144] and showed excellent rate performance (96 mAh g^{-1} at 20C) as anode. This performance comes partly from the fact that N doping is favorable to improve the electronic conductivity, and thus the rate capability [145]. Mesoporous single crystals $Li_4Ti_5O_{12}$

grown on reduced graphene oxide (MSCs-LTO-rGO) nanohybrids exhibited high specific capacity (171 mAh g^{-1}) with much improved rate capability (132 mAh g^{-1} at 40C) and cycling stability (85% capacity retention after 2000 cycles) [146]. TiO_2/graphene nanocomposite with well-preserved flower-like nanostructure formed by TiO_2 nanoparticles with a size of several nanometers delivered a capacity of 230 mAh g^{-1} at C/10 (corresponding to a density of 17 mA g^{-1}), and demonstrates superior high-rate charge-discharge capability and cycling stability at charge/discharge rates up to 50C [147]. The authors of this work went further by testing a full cell using this TiO_2/graphene as the anode material and spinel $LiMnO_2$ as the cathode material. Good high-rate performance and cycling stability were observed.

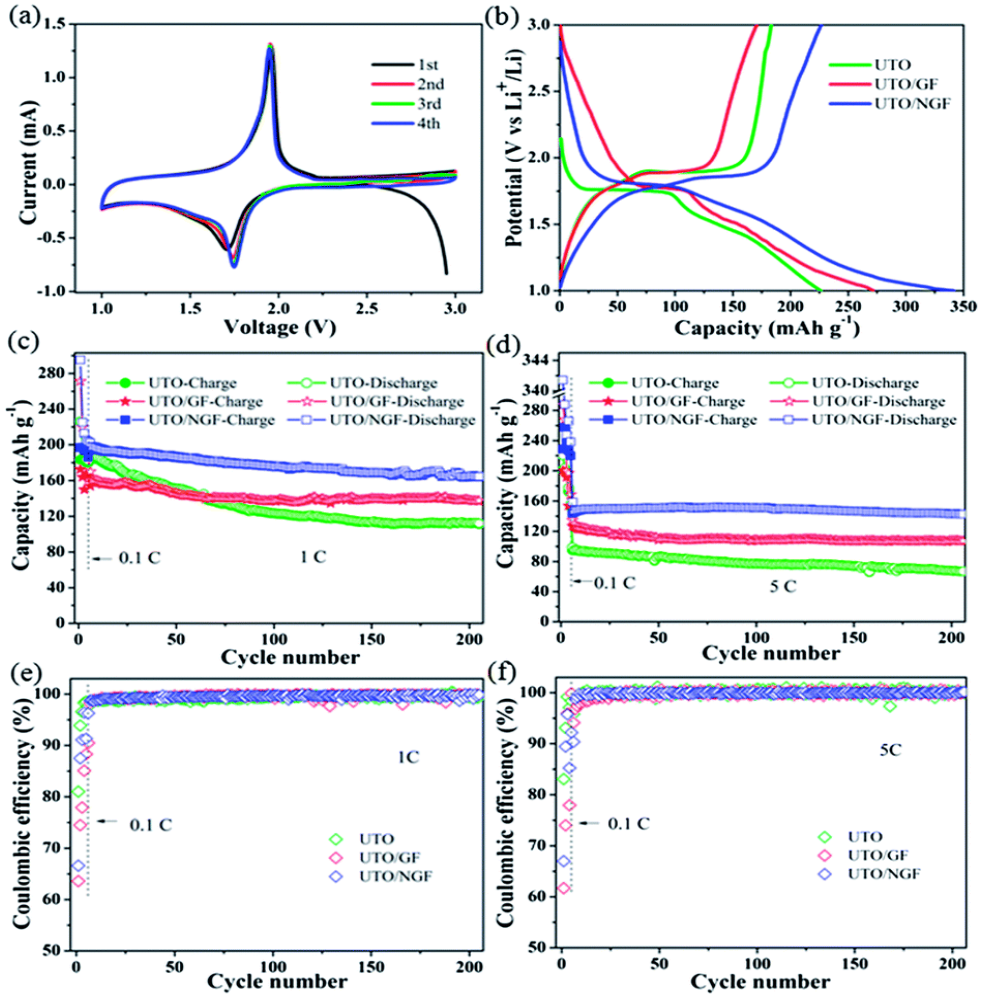

Figure 5. (a) Cyclic voltammograms of TiO_2 nanoparticles embedded in N-doped graphene networks (denoted as UTO/NGF) electrode between 1.0 and 3.0 V at a scan rate of 0.5 mV s^{-1} for the first four cycles. Initial charge−discharge curves of UTO, UTO/GF and UTO/NGF electrodes at a current density of 0.1C (1C = 168 mA g^{-1}). The comparative cycling performance of the above three electrodes: (c) 200 cycles at 1C after 5 cycles at 0.1C. (d) 200 cycles at 5C after 5 cycles at 0.1C. (e and f) The corresponding coulombic efficiency for (c and d), respectively (from Ref. [144]).

TiO_2 quantum dots (6 ± 2 nm)/graphene nanosheets (23.5 wt% graphene) retained a capacity of 190 mAh g^{-1} after 100 charge-discharge cycles at a current rate of 1C [148]. The increase of the C-rate to 10C leads only to an insignificant drop in capacity to 145 mAh g^{-1}. At 50C, the capacity was still 101 mAh g^{-1}. A composite consisting in 10 nm-thick TiO_2 nanotubes built on a graphene layer delivered a capacity of 350 mAh g^{-1} at the current density 10 mAh g^{-1}, 150 mAh g^{-1} after 50 cycles at the rate of 4 A g^{-1}, and 80 mAh g^{-1} after 2000 cycles at the rate of 8 A g^{-1} [149]. More recently, well-crystallized TiO_2 particles 6 nm in diameter were coated with amorphous carbon are anchored on reduced graphene oxide owing to post-treatment with UV irradiation [150]. This composite, as an anode, exhibited reversible capacities of 382 and 73 mAh g^{-1} at C/10 and 5C, respectively. The reversible capacity after 100 cycles at C/5 rate was 191 mAh g^{-1}. Better results, however, have been obtained on minky-dot-fabric-shaped composite of well-organized porous TiO_2 microspheres and reduced-graphene-oxide (rGO) sheets used as an anode delivered a reversible capacity of 100 mAh g^{-1} at 10C for up to 100 cycles [151]. Actually, the comparison between these different results illustrates that, in addition to the dispersion of the TiO_2 particles and their anchoring on the graphene sheets, the porosity is a crucial parameter that impacts the electrochemical properties of the TiO_2/graphene composites. For instance, mesoporous graphene nanosheets delivered a reversible capacity of 833 mAh g^{-1} after 60 cycles [152] owing to the increased effective surface area associated with the pores.

So far, all the data we have reported were obtained with anatase TiO_2. Another polymorph is rutile TiO_2, but very few composites formed with this polymorph have been tested as an anode for Li-ion batteries. Recently, however, rutile TiO_2 mesocrystals/reduced graphene oxide nanosheets exhibited a large capacity over 150 mAh g^{-1} at 20C after 1000 cycles, and high rate capability up to 40C [153].

The last polymorph is bronze (TiO_2-B), which is attractive, because of its fast kinetics illustrated by the results obtained with TiO_2-B microspheres with 12 nm pore size which retained a capacity of 149 mAh g^{-1} after 5000 cycles [154] at 10C rate. Carbon-coated TiO_2-B nanowires exhibited a capacity of 560 mAh g^{-1} after 100 cycles at current density 30 mA g^{-1} and 200 mAh g^{-1} when cycled at current density 750 mA g^{-1} [155]. A TiO_2-B/N-doped graphene porous nanocomposite with a high specific surface area of 163.4 m^2 g^{-1} showed a discharge capacity of 220.7 mAh g^{-1} at the 10C rate with a capacity retention of 96% after 1000 cycles. In addition, it can deliver a discharge capacity of 101.6 mAh g^{-1} at an ultra-high rate of 100C, indicating its great potential for use in high power lithium ion batteries [156]. A simple photocatalytic reduction method was used to simultaneously reduce graphene oxide (GO) and anchor (010)-faceted mesoporous bronze-phase titania (TiO_2-B) nanosheets to reduced graphene oxide (RGO) through Ti–C bonds. Owing to this Ti–C bonding, this composite delivered a specific capacity of 275 mAh g^{-1} at 1C rate and 200 mAh g^{-1} even at 40C current. Independent of the current densities, these electrodes maintained 80% of the initial capacity even after 1000 cycles [157]. Obviously, TiO_2-B is the polymorph that gives the highest rate capability. The specific capacity of TiO_2-based composites is smaller than that of Si-based composites, but the rate capability is much better, so that they both could find a market as anode materials.

Note, TiO_2 does not need to be crystallized to be electro-active, but the results are not good. Amorphous TiO_2 thin films uniformly deposited onto worm-like graphene nanosheets delivered a

stable capacity of ~140 mAh g^{-1} after 100 cycles at a specific current of 100 mA g^{-1} and accounted for a sustainable 95 mAh g^{-1} capacity at a specific current of 1200 mA g^{-1} [158].

Due to the smaller volume change during cycling, TiO_2 has been mixed with another metal oxide hoping to find a compromise taking advantage of the stability of TiO_2 upon cycling and the large capacity of the other component. Unfortunately, low cycle retention was witnessed for these TiO_2-based dual oxide anodes, e.g. TiO_2/Fe_2O_3 (capacity retention after 100 cycles at current density 200 mA g^{-1} ≈ 68%) [159], TiO_2/MnO_2 (≈60%) [160] or TiO_2/SnO_2 (≈52%) [161]. One exception is TiO_2/Fe_3O_4 that will be discussed in the section devoted to iron oxides.

In any cases, the process to make these composites is expensive and difficult to prepare at the industrial scale, and indeed, the only new anode that emerged on the market so far is another titanium oxide such as $Li_4Ti_5O_{12}$.

6.2. $Li_4Ti_5O_{12}$

All the metal oxides have in common the property of a huge volume change during cycling, with one exception: $Li_4Ti_5O_{12}$ (LTO), which explains the tremendous interest in this material considered as the "zero-strain" anode material, despite its much smaller theoretical capacity of 175 mAh g^{-1}. The rather high operational voltage of 1.55 V vs. Li^0/Li^+ that limits the tap density, but it also mitigate the formation of the SEI provided the voltage is maintained above 1 V, so that the cycling tests of LTO are usually performed in the voltage range 1.0–2.5 V. The structural stability is very good, and the LTO anode is safe.

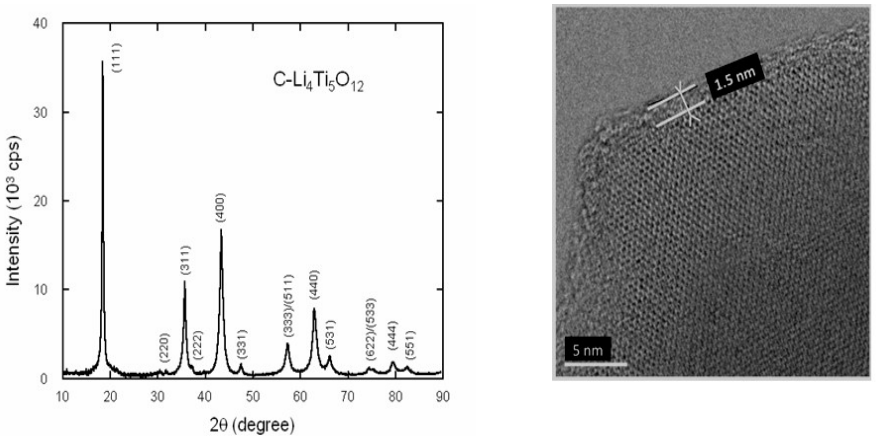

Figure 6. (a) Typical XRD patterns of C-$Li_4Ti_5O_{12}$ composite and (b) HRTEM image of a 90 nm sized LTO particle 1.5 nm carbon coating (from Ref. [163]).

The electrical conductivity is small (10^{-12}–10^{-13} S cm^{-1}), so that carbon-coating the LTO of any kind (particles, nanorods, hollow spheres) improves the electrochemical properties. 5 wt% C-coated 100 nm-sized LTO particles delivered a capacity of 165 mAh g^{-1} with 99% retention after 100 cycles at 1C rate [162]. Similar particles (same thickness 1.5–3.0 nm of the carbon coat, particles 90 nm in size (see Figure 6) were tested in a full 18650 cell with C-$LiFePO_4$ cathode [163]. The cell displayed a charge capacity of 650 mAh at low C-rate and retained more than 80% of rated capacity at 60C

charge rate. As shown in Figure 7. The reduction of the thickness of the carbon coat to 1 nm improves the diffusivity of the lithium through the coat and thus improves the rate capability as a capacity of 136 mAh g^{-1} at 20C rate has been reported for such a C-LTO composite [164].

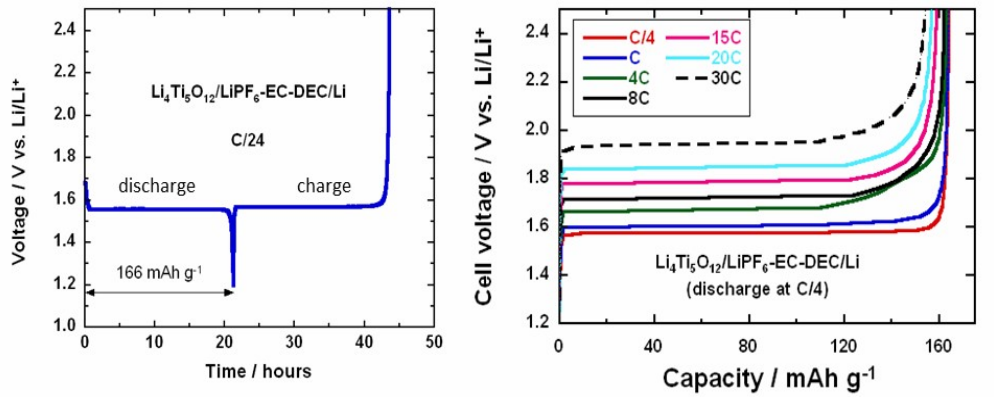

Figure 7. (a) Typical plateau of the discharge-charge curves of C-$Li_4Ti_5O_{12}$/1 mol L^{-1} $LiPF_6$ in EC-DEC/Li cell at C/4 rate. (b) Charge curves of C-$Li_4Ti_5O_{12}$/1 mol L^{-1} $LiPF_6$ in EC-DEC/Li cell at various C-rates (from Ref. [163]).

One strategy consisted in coating LTO with N-doped carbon instead of un-doped carbon, to take benefit of the doping effect on the electrical conductivity already mentioned in this review. The best results were obtained with 7 wt% N-doped carbon coated LTO spherical particles. At 2C rate, the initial capacity was 150 mAh g^{-1}, with a capacity retention of 83% after 2200 cycles [165]. Recently, 10 wt% hollow graphitized nano-carbon was used as a conductive agent, uniformly distributed on the surface of 50–100 nm-thick LTO particles providing 162 and 105.4 mAh g^{-1} at the rate of 15 mA g^{-1} and 1.5 A g^{-1}, respectively, and the discharge capacity retention rate after 500 cycles is 91.2% at 5C [166].

Another strategy to improve the performance was to use porous LTO to increase the effective surface area. C-coated porous LTO particles (pore diameter 4.3 nm) delivered 158 and 100 mAh g^{-1} at 1C and 50C rate, respectively, with good capacity retention [167]. These results are quite comparable with the prior results above mentioned for un-doped C-LTO, but the particles were much bigger: 0.5–1 μm instead of 90–100 nm. With smaller particles, even without carbon coating, spheric porous LCO particles of size 660 ± 30 nm, primary particle size of 20–100 nm, specific surface area of 15.5 m^2 g^{-1}, capacities of 179 mAh g^{-1} at 0.5C and 109 mAh g^{-1} at 10C were observed, with a capacity retention of 97.8% over 100 cycles [168].

Carbon nanotubes/LTO composites also gave good results [169,170]. Better results can be obtained by adding carbon. For a total 6 wt% carbon plus nanotubes, capacities of 163 and 143 mAh g^{-1} were reported at 0.5C and 10C rates, respectively. The capacity was stable at 146 mAh g^{-1} over 100 cycles at 5C rate [171]. The same capacity retention of 146 mAh g^{-1} over 100 cycles was observed, but at 10C-rate, in a LTO/multiwalled carbon nanotube (MWCNT) composite [172]. 50 nm-thick LTO particles anchored on MWCNTs for an amount of MWCNTs of 10 wt% delivered a capacity of 171 mAh g^{-1} and 90 mAh g^{-1} at 1C and 30C rate, respectively, stable

over the 30 cycles that have been tested [173]. Note, however, that this is comparable to the performance of the particles coated with n-doped carbon mentioned above, according to a synthesis process that seems more scalable. Again, still better results can be obtained with porous LTO. MWNT/LTO core/25 nm-thick sheet coaxial nanocables providing a surface area of 80 m^2 g^{-1} exhibited a capacity of 90 mAh g^{-1} over 100 cycles at 40C rate [174].

Only few works are related to LTO/graphene composites. A graphene-embedded LTO composite with 1wt% graphene gad a reversible capacity of 110 mAh g^{-1} at 22C rate. After 1300 cycles, a capacity of 101 mAh g^{-1} was maintained [175]. More recently, well-dispersed mesoporous LTO particles onto rGO delivered a reversible capacity of 193 mA h g^{-1} at 0.5C, 168 mAh g^{-1} at 30C between 1.0 and 2.5 V, owing to the addition of the improved electronic conductivity and buffering effect of the graphene, and the increased surface lithium storage capability brought by the porosity [176].

In an attempt to find a compromise between Si that has a very large capacity and LTO that has a very good rate capability, LTO/Si composites have been explored. with moderate Si contents (LTO:Si = 50:20) were the best compromise, delivering stable capacity (100 mAh g^{-1}) with good cycling performance, even at a very high current density of 7 A g^{-1} [177]. For the same reason, LTO/anatase TiO_2 composites have also been synthesized by the hydrothermal process [178,179,180]. Such a nano-composite with particles 30 nm-thick exhibiting rich hierarchical pores and a specific surface area of 91.88 m^2 g^{-1} delivered 150 mAh g^{-1} at 20C, and capacity retention of 151.4 mAh g^{-1} after 100 cycles at 1C [180].

7. Sulfides and Nitrides

7.1. Sulfides

7.1.1. SnS_2-based Composites

SnS_2 operates by a conversion reaction followed by alloying/de-alloying process (Eqs. 1–2). Only the second reaction is supposed to be reversible, but as usual in nanostructured materials, the experimental capacity can be larger because the surface offers new active sites resulting in higher than 4.4 Li per tin atom. For instance, layered SnS_2 nano-sheet arrays consisting of 1–5 atomic layers synthesized on Sn foil delivered 1050 mAh g^{-1} [181]. An Economical synthetic route for production of large-amounts (gram scale) of two-dimensional (2D) layered SnS_2 nanoplates showed good electrochemical performance, but was tested only for 30 cycles [182].

Composites composed of acetylene black adorned porous SnS_2 secondary microspheres that are assembled from a number of nanosheets with thicknesses of 20–50 nm (specific surface area of 129.9 m^2 g^{-1}) delivered 525 mAh g^{-1} at a current density of 400 mA g^{-1} over 70 cycles [183]. Mesoporous carbon anchored with SnS_2 nanosheets (14.3 wt% carbon) delivered a stable discharge capacity of 428.8 mAh g^{-1} after 50 cycles at current density 100 mA $g^{-1}$with a retention of 64.4% comparing with the first reversible capacity [184]. SnS_2 nanoflakes decorated multiwalled carbon nanotubes delivered 518 mAh g^{-1} at a current density of 100 mA g^{-1} between 5 mV and 1.15 V versus Li^0/Li^+. A stable reversible capacity of 510 mAh g^{-1} is obtained for 50 cycles [185]. These

results are an improvement with respect to pristine SnS_2 nanoflakes, pointing to the advantage of the composite, owing to the flexibility and the conductivity of the carbon nanotubes.

Balogun et al. demonstrated an effective strategy to improve the first reversible capacity and lithium storage properties of SnS_2 by growing SnS_2 nanosheets on porous flexible VN substrates [186]. The 3D porous VN coated SnS_2 nanosheets yielded a reversible capacity of 75% with high specific capacity of about 819 mAh g^{-1} at a current density of 0.65 A g^{-1}, decreasing to 791 mAh g^{-1} after 100 cycles. A capacity of 349 mAh g^{-1} was still retained after 70 cycles at current density of 13 A g^{-1}.

SnS_2/graphene nanosheets have been the subject of intense research these last years. Ce-SnS_2 crystal particles with a flower-like structure (particle sizes of each petal are in the range 50–100 nm) distributed on the graphene sheets delivered 707 mAh g^{-1} at C/2 after 50 cycles [187]. SnS_2 nanosheets linked with each other and dispersed uniformly on reduced graphene oxide surface delivered 896 mAh g^{-1} after 40 cycles at C/10 and 657 mAh g^{-1} after 40 cycles at 1C rate [188]. Few-layer SnS_2/graphene composite delivered a stable reversible capacity of 920 mAh g^{-1} at the 50th cycle at 100 mA g^{-1}, 600 mAh g^{-1} at 1 A g^{-1} [189]. Better results have been reported: SnS_2/graphene nanosheets delivered a capacity of 1114 mAh g^{-1} after 30 cycles at current density 100 mAh g^{-1}, and 870 mAh g^{-1} at current density 1 A g^{-1} [190]. A SnS_2@RGO nanocomposite consisting of 93.2 wt% SnS_2 and 6.8 wt% RGO delivered 564 mAh g^{-1} after 60 cycles at C/5 and 503 mAh g^{-1} at 2C [191]. SnS_2 nanosheets uniformly coating on the surface of graphene delivered a capacity of 570 mAh g^{-1} after 30 cycles at C/5 rate [192]. SnS_2 nanoplates with a lateral size of 5–10 nm are anchored on graphene nanosheets maintained a capacity of 704 mAh g^{-1} in the 100th cycle with charging at 1.6 mA cm^{-2} and discharging at 0.2 mA cm^{-2} [193]. Better results were obtained with a one-step hydrothermal route to prepare SnS_2/reduced graphene oxide nanocomposites (TSG) with hexagonal SnS_2 nanoplates (lateral size and thickness 140 nm and 25 nm) and nanocrystals (6 nm-thick) [194]. As an anode, this composite delivered 1005 mAh g^{-1} after 200 cycles at the current density of 100 mA g^{-1} and 612 mAh g^{-1} at the rate of 2 A g^{-1}. This result is due to the fact that this composite takes benefit not only on the synergistic effect between SnS_2 and graphite, but also of the porosity (average pore size 5.37 nm, surface area 77.8 m^2 g^{-1}. $SnSn_2$ nanocrystals (lateral size of 3–4 nm) decorated on flexible reduced graphene oxide delivered 1034 mAh g^{-1} after 200 cycles at C/10, 737 mAh g^{-1} after 200 cycles at 1C, and the capacity after 450 cycles was maintained at 570 mAh g^{-1} (3C) and 415 mAh g^{-1} (5C), respectively [195]. SnS_2 nanoplates ca. 7 nm-thick/graphene composite exhibited a reversible capacity stable at ca. 668 mAh g^{-1} after 10 cycles at a rate of 100 mA g^{-1} and 480 mAh g^{-1} at 1600 mA g^{-1} [196]. The best result, however, was reported on 3D porous graphene networks anchored with Sn nanoparticles (5–30 nm) encapsulated with graphene shells of about 1 nm. As an anode, this composite exhibited very high rate performance. The capacity reached 682 mAh g^{-1} at the rate of 2 A g^{-1} and remained approximately 96.3% (657 mAh g^{-1}) even after 1000 cycles [197].

Among SnS_2/graphene aerogels, the best result reported a capacity of 656 mAh g^{-1} with a coulombic efficiency of over 95% after 30 cycles and 240 mAh g^{-1} at the rate of 1000 mA g^{-1} [198]. Other Sn-based composites have also been reviewed in [199].

A Cu_6Sn_5-Cu_3Sn-CNTs composite anode showed a good cycling performance, with a capacity 513 mAh g^{-1} after 100 cycles at 1C rate, and a good rate capability, with a capacity of 411 mAh g^{-1} at 16C rate [200].

7.1.2. Titanium Sulfides

TiS_2 has a high conductivity, low cost and light weight. Unfortunately, it suffers irreversible changes including passivation of the surface and distortion of the chemical structure. Nevertheless, it has excellent cycling performance between 3.0 and 1.4 V. Particle pulverization and formation of Li_2S lead to performance degradation because of the irreversible dissolution of Li_2S into the electrolyte below 0.5 V [201]. TiS_2-multi-walled carbon nanotubes (MWCNTs) (1:1) composite delivered an initial capacity of 450 mAh g^{-1} with 80% capacity retention after 50 cycles owing to the synergetic effect between TiS_2 and the MWCNTs [202]. However, TiS_2 like MoS_2 suffers from the rather high working potential (in the 2–V range) with respect to the Li^0/Li^+ redox potential, which reduces significantly the energy density of the battery. As a consequence, TiS_2 and MoS_2 are considered as so that they are now placed in the category of 2-volts cathode materials, not as promising anode elements [203].

7.1.3. Nickel Sulfides

Nickel sulfides NiS, NiS_2, Ni_3S_2, and Ni_3S_4 have gained special attention as electrode materials for lithium-ion batteries and super-capacitors [204]. In particular, NiS has attracted attention, owing to its high theoretical capacity of 590 mAh g^{-1}. As usual, various carbonaceous materials to support NiS anodes to buffer the volume change of NiS and increase the electrical conductivity.

Nickel sulfide-carbon core-shell composite powders were prepared by a one-step spray pyrolysis, where the nickel sulfide particles were of submicron size, and crystallized in the Ni_7S_6 phase. As an anode, this composite delivered a discharge capacity of 472 mAh g^{-1} at a high current density of 1000 mA g^{-1}, even after 500 cycles [205].

NiS-carbon fiber composite electrodes coated with Li_2S-P_2S_5 solid electrolytes by pulsed laser deposition (PLD) delivered a capacity of 300 mAh g^{-1} at the 50th cycle at current density 3.8 mA cm^{-2} corresponding to approximately 1C rate [206]. This coating was thus able to form avorable lithium ion and electron conduction paths for the NiS active materials. Another NiS (50 nm diameter)-carbon fiber composite retained a discharge capacity of 520 mAh g^{-1} and a charge-discharge efficiency of approximately 100% after 30 cycles in the voltages of 0–4.0 V vs. Li^0/Li^+ under a constant current density of 1.3 mA cm^{-2} [207].

Camphoric carbon wrapped NiS powders were prepared in a morphology showing a network of interconnected nanoscale units with rod like profiles, which terminated into needle-like apexes spanning diameters of about 50–80 nm with BET surface area of 32 m^2 g^{-1} [208]. As an anode, this composite delivered a specific capacity reduced from 290 mAh g^{-1} to 225 mAh g^{-1} (20%) after the 100th cycle from 3.2 V to 0.5 V at current density 5 mA g^{-1}.

The morphology, size and phase control of NiS nanoflowers on a graphene substrate was investigated in [209]. The best result was obtained with graphene supported NiS nanorod-assembled nanoflower that delivered a capacity of 887 mAh g^{-1} after 60 cycles at 59 mA g^{-1}, much larger than the theoretical capacity of NiS (590 mAh g^{-1}). These good results show that prevention of graphene agglomeration could be preserved during repetitive cycling. A NiS/graphene (NiS/G) nanohybrid was synthesized by a facile in situ one-pot hydrothermal route in a sheet-on-sheet structure, where

ultrathin NiS sheets (below 5 nm) are anchoring on few-layer (below 8 layers) graphene sheets [210]. This composite cycled between 0.05 V and 3.0 V at 50 mA g^{-1} retained a charge capacity of 481 mAh g^{-1} after 100 cycles. At a current density of 800 mA g^{-1} (1.5C rate) NiS/G still yielded a charge capacity of 386 mAh g^{-1}.

Ni_3S_2 nanobowls with an average size of 250 nm and shell thickness of 30 nm wrapped by reduced graphene oxide sheets 43 mAh g^{-1} at 0.5C after 500 cycles (theoretical capacity of Ni_3S_2 is 462 mAh g^{-1}) [211]. The improved cycle stability of the composite could be ascribed to the bowl structure with both exposed interior and exterior arch surfaces which could stand much more lithiation-delithiation than quasi-1D hollow chains.

Activated cotton textile (ACT) with porous tubular fibers embedded with NiS_2 nanobowls and wrapped with conductive graphene sheets (ACT/NiS2-graphene) retained a capacity of 645 mAh g^{-1} at 1C after 100 cycles recovered to <1016 mAh g^{-1} at C/10 after 400 cycles [212]. Sphere-like NiS_2 particles/graphene composite delivered a capacity of 1200 mAh g^{-1} at the 120th cycle current density 100 mA g^{-1} and about 810 mAh g^{-1} at a current density of 500 mA g^{-1}. After 1000 cycles at a current density of 500 mA g^{-1} this NiS_2/graphene composite still preserved a capacity of 810 mAh g^{-1}, indicating its excellent cyclic stability, an evidence that the reduced graphene oxide efficiently restrained NiS_2 from agglomerating during hydrothermal synthesis [213].

With its high theoretical capacity (704.5 mAh g^{-1}), safety and low cost, Ni_3S_4 is also a promising candidate as an anode. Ni_3S_4-nitrogen doped graphene composite showed outstanding performance with 98.87% capacity retention from 2nd (1338.4 mAh g^{-1}) to 100th (1323.2 mAh g^{-1}) discharge cycle at 0.2C in the range of 0–3 V [214]. A capacity of 793.9 and 558.2 mAh g^{-1} stable over 100 cycles was observed at 2C and 4C rate, respectively. The authors attributed this performance to the fact that nitrogen-doping process introduced disordered carbon and lithium intercalated active sites. Also the annealing at 250 °C increased the grafting of the Ni_3S_4 particles on the graphene, thus increasing the conductivity, and increased the percentage of pyridinic nitrogen, which is more effective to enhance the reversible capacities of graphene than other types of nitrogen [215]. This attribution of the improvement of the electrochemical properties to the graphene and its N-doping is confirmed by the good performance of $NiS_{1.03}$-nitrogen doped graphene composite prepared in the same conditions, which showed 95.94% capacity retention from 2nd (1084 mAh g^{-1}) to 100th (1040 mAh g^{-1}) cycle discharge at 0.2C rate.

7.1.4. Cobalt Sulfides

Cobalt sulfides also have promising potential as a high capacity, high rate and long life anodes. The growth of a carbon shell on hollow nanospheres of mesoporous Co_9S_8 improved the reversible capacities at high rates: 896 mAh g^{-1} after 800 cycles at 2 A g^{-1} [216]. Carbon-coated Co_9S_8 nanodandelions delivered a specific capacity of 520 mAh g^{-1} at a current density of 1 A g^{-1} (1.8C) during the 50th cycle (against 338 mAh g^{-1} without carbon coating) and a 10th-cycle capacity of 373 mAh g^{-1} at a current density of 6 A g^{-1} (10.9C) [217].

Graphene-wrapped CoS nanoparticles delivered a delivered a specific capacity of 749 mAh g^{-1} after 40 cycles at 62.5 mA g^{-1} or 550 mAh g^{-1} after 100 cycles at 312.5 mA g^{-1} [218].

7.1.5. Iron Sulfides

FeS_2 has been less studied than other sulfides, although its theoretical capacity is high (894 mAh g^{-1}). Promising results were obtained with carbon-coated FeS_2 particles composed of rod-like second particles with diameters of 0.2–1μm and lengths of 0.5–3 μm, the rod-like second particles being made up of small first nanoparticles with 30–100 nm in diameters. The pores between the nanoparticles are 5–30 nm in size [219]. The specific reversible capacity of this FeS_2/C composite after 50 cycles is 495 mAh g^{-1} at 0.05 C and 371 mAh g^{-1} at 0.2C, respectively.

FeS_2 decorated sulfur-doped carbon (FeS_2@S-C) fibers have been successfully synthesized by a facile bio-templating method. As an anode, this composite retained a high reversible specific capacity of 689 mAh g^{-1} after 100 cycles at current density of 0.1 A g^{-1} [220]. After 10 cycles at 2 A g^{-1} the capacity was 400 mAh g^{-1}. A composite of reduced graphene oxide and FeS_2 microparticles maintained a capacity of 1001 mAh g^{-1} over 60 cycles at a current rate of 100 mA g^{-1} [221]. Nevertheless, FeS_2 severs from irreversible reactions elucidated in [222], which results in aging of the material and reduces the capacity along cycling. In addition, two charge plateaus at about 1.8 V and 2.4 V are clearly shown at the first charge process, followed by two discharge plateaus at about 1.55 V and 2.05 V, due to the conversion of metallic Fe to FeS and oxidization of Li_2S through lithium polysulfide to sulfur, respectively. The following discharge plateaus are their corresponding reverse processes. According to these rather high voltages, FeS_2 can be considered either as a cathode of the 2-V family [223] rather than as an anode with a limited energy density.

7.2. Nitrides

Transition metal nitrides possess fair electrical conductivity but superior chemical stability, which qualify them for candidates for supercapacitors or electrodes for Li-ion batteries. In particular, Nb_4N_5 nanochannels electrode with an ultrathin carbon coating exhibits an areal capacitance 243.6 mF cm^{-2} at 0.5 mA cm^{-2}, with nearly 100% capacitance retention after 2000 CV cycles [224]. Due to the fast diffusion of Li ions as a result of the Li vacancies after the conversion reaction, metal nitrides also offer the possibility to reach relatively high power densities [225]. Except $LiMoN_2$ that is a cathode material in a voltage range of 2.7–4.2 V, the newly developed lithium layer nitrides were anodes because their Li intercalation voltage plateau lies below 2 V. A recent review on metal hydrides as high performance anode materials for lithium-ion batteries can be found in [226], where the reader will find their intrinsic properties. We are interested here on the improvement obtained by their integration in composite materials.

7.2.1. Carbon and Silicon Nitrides

Attempts are currently made to use carbon nitride to enhance the stability of the SEI and also act as a buffer layer for the volume change of the active materials during cycling, since strong covalent bonds between carbon and nitride leads to materials highly resistant against the corrosion by the electrolytes while the high electrical conductivity is maintained by the conjugative π structure which is similar to graphite. In addition, Li^+ uptake for 10% graphitic carbon nitride is similar to a graphite

electrode, indicating that it does play a role in determining the storage capacity of graphitic carbon nitride-based composites as anode materials for Li-ion batteries [227]. Nanowire arrays of CuO followed by deposition of ultrathin carbon nitride (CN_x) films through radio-frequency sputtering of a graphite target in a high-purity N_2 gas formed 3D CuO/CN_x core-shell nano-architectures that delivered a capacity of 669 mAh g^{-1} after 200 cycles at current density 50 mA g^{-1} [228]. Graphitic carbon nitride (g-C_3N_4) uniformly coated on SnO_2-TiO_2 nanoparticles displayed a capacity of 380.2 mAh g^{-1} at 0.2C rate after 20 cycles and 330 mAh g^{-1} at 0.5C [229]. Let us recall the good performance of a hybrid of graphitic carbon nitride with reduced graphene oxide [38]. Instead of carbon nitride, silicon nitride was also used as a coating material. In particular, it was shown that a silicon nitride coating of silicon thin films has a positive effect on both the cycling stability and high rate performance [230].

7.2.2. Vanadium Nitride

Vanadium nitride (VN) nanowires possess obvious pseudocapacitive characteristics with a very low redox potential (0.01–3V vs. Li^0/Li^+), and can get further gains in energy storage with the assistance of graphene so that it is a promising anode material [231]. In particular, by employing such VN/reduced graphene oxide composite and porous carbon nanorods with a high surface area of 3343 m^2 g^{-1} as the anode and cathode, respectively, a novel hybrid Li-ion was fabricated, with an ultrahigh energy density of 162 Wh kg^{-1} at 200 W kg^{-1}, which also remains 64 Wh kg^{-1} even at a high power density of 10 kW kg^{-1}. The specific capacity was 640 mAh g^{-1} at 0.1 A g^{-1} [231]. Vanadium nitride and nitrogen-doped graphene nanosheet (G) hybrid materials showed an initial coulombic efficiency 74.6%, while that of the pristine VN was only 55.8% [232], illustrating that the combination of such binder free materials and metal nitrides increases the conductivity of metal nitrides [233].

7.2.3. Titanium Nitrides

Titanium nitride nanowires on carbon textiles supported Si nanofilms investigated as anodes without using binders and conductive additives delivered a capacity of 3258.8 mAh g^{-1} with a discharge capacity retention of 94.7% after 200 cycles at a current density of 1 A g^{-1}, an important improvement with respect to the performance obtained with TiO_2 instead of TiN [234]. TiN-coated $Li_4Ti_5O_{12}$ nanocomposites with different mass ratios exhibited markedly improved electrochemical propertieswith respect to pristine $Li_4Ti_5O_{12}$ as it exhibited a capacity of 130 mAh g^{-1} at a charge/discharge rate of 20C and a capacity retention 85% after 1000 cycles at 10C [235]. A result comparable to the VN/N-doped graphene composite in [233] was reported for another binder free graphene/titanium nitride hybrid material [236]. This G/TiN hybrid anode exhibits a reversible capacity as high as 325 mAh g^{-1} at current rate 2000 mA g^{-1}, much higher than that of pure graphene at 98 mAh g^{-1} after about 35 cycles.

7.2.4. Other Transition Metal Nitrates Composites

A NbN nanoparticle/nitrogen-doped graphene composite was explored as a new anode with a

high energy density of 123 Wh kg^{-1} [237]. 81.7% capacity retention after 1000 cycles at 0.5 A g^{-1} was obtained.

Zheng et al. modified the surface of Fe_3O_4 nanoparticles with Fe_3N [238]. A reversible capacity over 739 and 620 mAh g^{-1} was obtained after each 60 cycles at a current density of 50 and 200 mA g^{-1}, respectively for this Fe_3O_4@Fe_3N composite.

In the same way, nanocoating of Mo_2N on the surface of hollow-nanostructured MoO_2 is highly effective in improving the conductivity of MoO_2 compared to the bare MoO_2 [239]. At a current density of 100 mA g^{-1}, this composite delivered a capacity of 815 mAh g^{-1} after 100 cycles. At very high current density of 5 A g^{-1}, the capacity was still 415 mAh g^{-1} (three times the capacity in absence of Mo_2N coating). In addition, these results were obtained without any binder, i.e. Mo_2N is the binder.

Mn_3N_2 has been proposed as a novel anode in 2012 [240]. The irreversible electrochemical reaction mechanism results in an unavoidable capacity loss and low columbic efficiency of 70% in the first cycle. Nevertheless, at 160 mA g^{-1}, the discharge capacity was 365.4 mAh g^{-1} after the 300th cycle. The main process in all the charge processes can be characterized by one slope plateau at around 1.1 V. These results show that this nitride is a promising anode material. Since then, carbon coated MnO@Mn_3N_2 core-shell composites (MnO@Mn_3N_2/C) were synthesized in a simple approach by calcinating MnO_2 nanowires with urea at 800 °C under an ammonia atmosphere. Urea derived carbon nanosheets were partially coated on pure phase MnO@Mn_3N_2 core-shell composites [241]. After 60 cycles with current density constantly changing, the reversible capacity of MnO@Mn_3N_2/C still remained above 626 mAh g^{-1} with a current density of 100 mA g^{-1}, exhibiting a significantly improved performance in comparison with the MnO/C and Mn_3N_2/C samples.

8. Conversion Anode Composites

The conversion reaction in transition metal oxides involves the formation of Li_2O according to the reaction:

$$MO + 2\ Li^+ \rightarrow M + Li_2O, \tag{4}$$

with M = Mn, Fe, Ni, Co, Cu. The first discharge reaction results in the amorphization of the lattice followed by the formation of nanoparticles of metal M embedded into the Li_2O matrix. In the charge reaction, Li_2O decomposes, and MO is reformed.

8.1. CoO-based Composites

Due to its low electrical conductivity and important volume changes upon cycling, good results with CoO as an anode can be obtained only in composites. Among the hybrid coated CoO particles, an unsealed hollow porous CoO shell with a Co metal core with avoid between the shell and the core delivered a capacity of 800 mAh g^{-1} after 70 cycles at current density 50 mA g^{-1} [242]. The same result was found for a carbon-decorated CoO composite, but at current density 100 mA g^{-1} [243]. Better results were obtained with CoO/$NiSi_x$ core-shell nanowire arrays, which delivered a reversible capacity of 600 mAh g^{-1} at 1C rate, and 400 mAh g^{-1} at 44C rate [244]. The deposition of CoO onto Cu nanaorods form nano-structures electrodes that delivered a reversible capacity of 900 mAh g^{-1}

after 200 cycles at current density 215 mA g^{-1} (0.3C) [245]. In a Co-Li_2O@Si core-shell nanowire array, the coated Si shell could be electrochemically active, while the Co-L_2O nanowire core could function as a stable mechanical support and an efficient electron conducting pathway during the charge-discharge process. The Co-Li_2O@Si core-shell nanowire array anodes exhibited good cyclic stability and high power capability compared to planar Si film electrodes [246].

CoO/graphene composites were studied because the graphene nanosheets function as a robust matrix increasing the conductivity of the CoO composite, but also buffering the large volume swings of the active CoO composite during the charge-discharge process. However, to avoid the aggregation of CoO nanoparticles, the practical applications of graphene-based materials in energy fields often require the assembly of 2D reduced graphene oxides sheets into 3D architectures [247]. After 100 discharge/charge cycles at 50 mA g^{-1}, the reversible capacities of a CoO/3D graphene nanocomposite remained 860 mAh g^{-1}. At 500 mA g^{-1}, the composite electrode was capable of delivering a stable capacity of about 391.2 mAh g^{-1} [248]. In another work, CoO/graphene composites with a mass ratio 9:1 exhibited a capacity of 1400 mAh g^{-1} over 60 cycles at current density of 100 mA g^{-1}, and still 500 mAh g^{-1} at 8 A g^{-1} [249]. This result is better than the performance exhibited previously by CoO/graphene nanosheets [250]. However, CoO quantum dots (3–5 nm) on graphene nanosheets were able to deliver 1592 mAh g^{-1} and 1008 mAh g^{-1} after 50 cycles at current density 50 mA g^{-1} and 1000 mA g^{-1}, respectively [251]. At last, 5 nm-thick CoO particles densely anchored on graphene sheets maintained a stable capacity of 1015 mAh g^{-1} for 520 cycles [252].

8.2. NiO-based Composites

Due to low cost, safety and low toxicity, NiO is considered as a promising anode for Li-ion batteries. The anode proceeds by the reversible conversion reaction:

$$NiO + 2\ Li^+ + 2\ e^- \rightarrow Ni^0 + Li_2O, \quad (6)$$

providing a theoretical specific capacity of 718 mAh g^{-1}.

The first lithiation occurs at 0.6 V, the subsequent ones slope from 1.0 to 1.4 V. However, the larger delithiation potential ranging from 1.5 to 2.2 V makes NiO less attractive since higher potential means less energy density. Nevertheless, it can be coupled with a high voltage cathode such as $LiNi_{0.5}Mn_{1.5}O_4$ electrode [253]. Like the previous materials already reviewed, it gives poor results, unless it is nanostructured; the porosity also plays an important role. The best result obtained for NiO used as an anode was reported for three-dimensional "curved" hierarchical mesoporous NiO nano-membranes, which delivered a capacity of 721 mAh g^{-1} at rate 1.5C and a lifetime of 1400 cycles [254]. Nanoporous NiO films directly grown on the foam Ni delivered a capacity of 543 mAh g^{-1} after 100 cycles at rate C/5, and showed a reversible capacity of 280 mAh g^{-1} at 10C rate [255]. Composites have been built to avoid the barrier that a uniform coat of NiO with a metal could rise for lithium transport. In particular, a composite NiO/Co-P composed of 200 nm-thick NiO particles and 30 nm-thick granular particles of Co-P delivered capacities of 560 and 270 mAh g^{-1} at current density 200 and 1000 mA g^{-1} [256].

Good results have been obtained with NiO: graphite composites, but the results depend very much on the architecture of the electrode, and also the amount of carbon. For instance a sandwich of

graphene nanosheets/NiO nanosheets delivered a capacity of 1030 mAh g^{-1} after 50 cycles at 0.5C rate, and retained 492 mAh g^{-1} at 5C; however the C/NiO was very high: 77.2:22.8 [257]. Improved rate capability was obtained with NiO/graphene nanosheet hierarchical structure prepared by electrostatic interaction between negatively charged graphene oxide and positively charged NiO in aqueous solution with pH = 4 [258], with a capacity of 615 mAh g^{-1} at a current density of 1.6 A g^{-1} (5.6C rate). In 2012, for almost the same current density 1.5 A g^{-1}, the capacity was raised to 727 mAh g^{-1} with reduced graphene oxide and nanosheet-based NiO microsphere composite [259]. In 2014, a core-shell Ni/NiO nanocluster-decorated graphene delivered 863 mAh g^{-1} after 300 cycles at current density 1.5 A g^{-1}, and 700 mAh g^{-1} after 40 cycles at current density 3 A g^{-1} [260]. Finally, in 2016, hierarchical NiO/Ni nanocrystals covered with a graphene shell were obtained with the hollow ball-in-ball nanostructure intact [261]. This NiO/Ni/graphene composite delivered a high reversible specific capacity of 1144 mAh g^{-1}, 962 mAh g^{-1} after 1000 cycles at 2A g^{-1} and an average capacity of 805 mAh g^{-1} at current density 15 A g^{-1}. This illustrates the fast improvement of the electrochemical performance of NiO-graphene composites through the recent years.

8.3. MnO-based Composites

MnO has a high theoretical capacity of 755 mAh g^{-1}, high density (5.43 g cm^{-3}), and is abundant. The application as an anode, however, is still hindered by the same characteristics as any conversion anode elements: large volume change during cycling, low electrical conductivity. Carbon-coated MnO prepared by ball-milling with sugar and pyrolysis at 600 °C exhibited a capacity retention of 650 mAh g^{-1} over 150 cycles at 0.08C. [262]. Increasing the sintering temperature whenever it does not damage the electrochemical-active material is a good idea because the conductivity of the carbon will be improved. 20 nm-thick MnO particles coated with carbon at 700 °C delivered a capacity of 939 mAh g^{-1} after 30 cycles at C/10 rate [263]. Porosity also helps, as usual with all the metal oxides. Porous carbon-coated MnO microspheres prepared at the same temperature delivered 700 mAh g^{-1} at current density of 50 mA g^{-1} over 50 cycles, and 400 mAh g^{-1} at 1.6 A g^{-1} [264]. A breakthrough has been achieved with new porous carbon-coated MnO spherical particles of size 300 nm [265]: this composite delivered a capacity of 1210.9 mAh g^{-1} after 700 cycles at 1.0 A g^{-1}.

Hollow structures also helped to accommodate the volume change during cycling of MnO. Hollow MnO/C microspheres delivered 700 mAh g^{-1} after 50 cycles at current density 100 mA g^{-1} [266]. Decreasing the size of the hollow spheres to the nano-range, and adding the porosity of the shell, the capacity could be raised to 1515 mAh g^{-1} after 60 cycles at current density 100 mA g^{-1}, and 1050 mAh g^{-1} after 100 cycles at current density 100 mA g^{-1} as shown in Figure 8 [267]. MnO nanocrystals embedded in 100–200 nm-thick carbon nanofibers obtained with a porous structure delivered 1082 mAh g^{-1} after 100 cycles at current density 100 mA g^{-1} and 575 mAh g^{-1} after 200 cycles at current density 1 A g^{-1} [268].

MnO/graphene composites were also synthesized, delivering a capacity of 2014 mAh g^{-1} after 150 cycles after 150 cycles at current density 200 mA g^{-1}, 843 mAh g^{-1} after 400 cycles at current density 2 A g^{-1} with only 0.01% capacity loss per cycle [269].

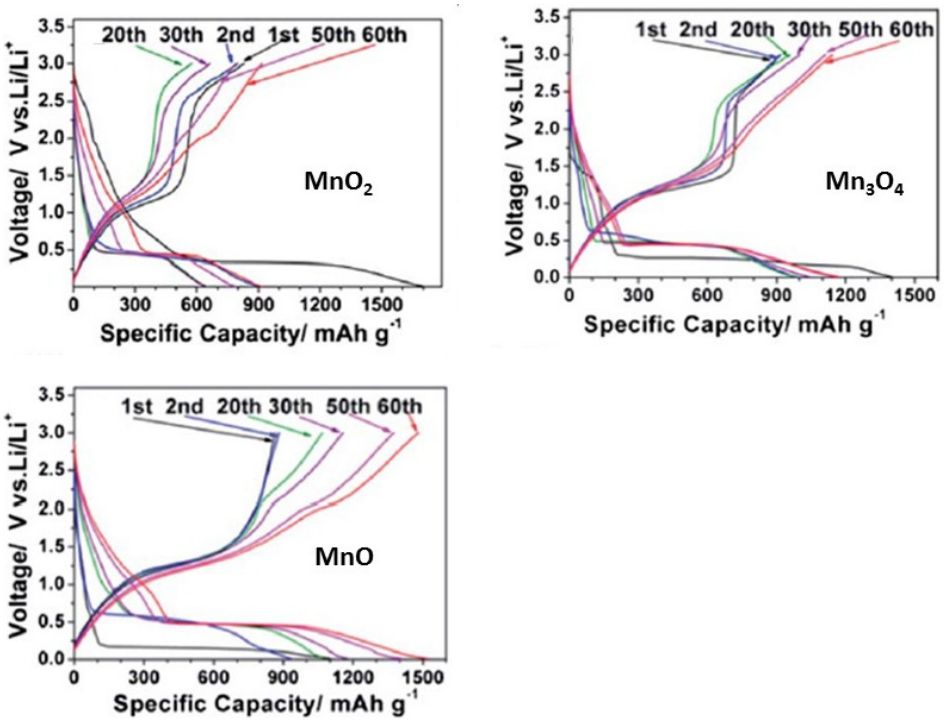

Figure 8. Comparison between discharge-charge curves of hollow MnO_2, Mn_3O_4 and MnO nanospheres as anode materials for lithium ion batteries. Cycling was carried out at current density 100 mA g^{-1} (from Ref. [267]).

We can thus conclude that there are now porous nanostructures of MnO either carbon-coated or anchored on graphite that have a long cycling life high capacity and good rate capability. The problem of deficiency of regularity in the structure and the limited elasticity of the shell material that were at the origin of the aging of the MnO-based composites [270] is definitely solved.

8.4. MnO_2-based Composites

MnO_2 has a higher theoretical capacity of 1232 mAh g^{-1}. It is thus logical that many efforts have been made to make MnO_2/C composites in parallel to the work made on MnO/C composites. Nano-urchin structure consisting of spherical onion-like C and MnO_2 nanosheets could deliver a reversible capacity of 404, 263, 178 and 102 mAh g^{-1} at rates of 200, 500, 1000, and 2000 mA g^{-1} [271].

MnO_2 nanoflakes coated on carbon nanohorns exhibited a capacity of 565 mAh g^{-1} at current density 450 mA g^{-1} [272]. Caterpillar-like nanoflaky MnO_2/carbon nanotuber delivered 801 mAh g^{-1} (<1000 mAh g^{-1} can be attributed to the MnO_2 porous layer alone) for the first cycle without capacity fade for the first 20 cycles [273]. Mesoporous γ-MnO_2 particles/single-walled carbon nanotubes composites maintained a capacity of 934 mAh g^{-1} over 150 cycles [274].

Graphene-MnO_2 nanotube as anode delivered a reversible specific capacity based on electrode composite mass of 495 mAh g^{-1} at 100 mA g^{-1} after 40 cycles; the capacity was 208 mAh g^{-1} at 1.6 A g^{-1} [275]. Graphene-Wrapped porous MnO_2-Graphene Nanoribbons maintained a specific

capacity of 612 mAh g^{-1} after 250 cycles at 400 mA g^{-1} [276]. MnO_2/3D porous graphene-like (62.7 wt% MnO_2, effective surface area 58 m^2 g^{-1}, total volume 0.2 cm^3 g^{-1}) delivered a discharge capacity of 988 mAh g^{-1} at the second cycle and the discharge capacity remained at 836 mAh g^{-1} at the 200th cycle at current rate 100 mAh g^{-1} and the capacity remained at 433 mAh g^{-1} at current density 1.6 A g^{-1} [277].

8.5. Mo Oxide-based Composites

Two Mo oxides have been investigated as anodes for Li-ion batteries: MoO_2 and MoO_3. Both of them have a good theoretical capacity that exceeds that of graphite: 838 mAh g^{-1} for MoO_2 and 1111 mAh g^{-1} for MoO_3. They share with the other metal oxides the same feature, i.e. the large volume change during cycling, and lo electrical conductivity, implying the use of composites to buffer the volume change, and increase the conductivity. In addition, they suffer from the fact that the conversion reaction is very slow, which limits the rate capability, reinforcing the need to decrease the size of the material to the nano-range.

Carbon-MoO_2 composites have improved the electrochemical properties with respect to bare MoO_2. A composite consisting in MoO_2 nanofibers coated with a 3 nm-thick carbon layer exhibited capacities of 762.7 mAh g^{-1} at 50 mA g^{-1} and 430.6 mAh g^{-1} at 200 mA g^{-1} with a columbic efficiency of nearly 100%, steadily retained after 50 cycles [278]. MoO_2/C nanospheres with diameters of about 15–25 nm were interconnected to form a cage-like architecture delivered a capacity of 692.5 mAh g^{-1} after 80 charge-discharge cycles at a current density of 200 mA g^{-1} [279].

The specific capacity of MoO_2/C hybrid nanowires at current density of 1 Ah g^{-1}, was retained at 327 mAh g^{-1}, i.e. 92% of that in the first cycle, after 20 cycles of discharge and charge [280]. An improvement of the rate capability has been obtained with MoO_2-Ordered Mesoporous Carbon Nanocomposite where ordered mesoporous carbon aggregates consisted of micrometer-sized rod-like particles. As an anode, this composite attained capacity of 401 mAh g^{-1} at a current density of 2 A g^{-1} [281]. Porosity can also compensate for an increase of the size of the structure from nano to micro range. Porous 2 μm sized MoO_2/Mo_2C/carbon sphere composites with BET surface areas the order of 155 m^2 g^{-1} delivered discharge capacities of 650 mAh g^{-1} after 100 cycles at current density 500 mAh g^{-1} [282].

MoO_2/graphene composites were also an improvement. A MoO_2/graphene oxide composite delivered a capacity of 720 mAh g^{-1} and 560 mAh g^{-1} after 30 cycles at a current density of 100 mA g^{-1} and 800 mA g^{-1}, respectively [283]. MoO_2 nanocrystallites of ca. 30–80 nm were wrapped in graphene layers and assembled into the secondary rods [284]. For this composite, the capacity reaches 407.7 mAh g^{-1} after 70 discharge and charge cycles at current density 2A g^{-1}. In another case, MoO_2-graphene electrode with graphene content 10.4 wt% showed a capacity of 1009.9 mAh g^{-1} after 60 charge/discharge cycles at a current density of 100 mA g^{-1} in the potential range 0.01–2.5 V [285]. When the current density is raised to 500 mA g^{-1}, the electrode can still deliver a charge capacity of 519 mAh g^{-1} up to 60 cycles. Note that these results are comparable with those obtained with layered MoS_2/CN-G composite anode that delivered a capacity of 800 mAh g^{-1} with great cycling stability [286].

MoO_3 has been investigated for many applications. For instance, redox Active

Polyaniline-h-MoO_3 hollow nanorods [287], ordered mesoporous α-MoO_3 with iso-oriented nanocrystalline walls [288], and ultrathin MoO_3 nano-crystals self-assembled on graphene nanosheets [289] were proposed as new supercapacitors. As an anode material, MoO_3 not only has a superior theoretical specific capacity of nearly 1111 mAh g^{-1} but also has a very stable one-dimensional (1D) layered structure. Recently, single-crystalline α-MoO_3 nanobelts prepared in 5 mol L^{-1} HNO_3 delivered a capacity of 175 mAh g^{-1} at the first cycle at 2C rate, falling to 150 mAh g^{-1} after 10 cycles, while commercial MoO_3 delivers a stable reversible capacity of 72 mAh g^{-1} at 2C rate [290]. To overcome the degradation of MoO_3 nanorod anodes in lithium-ion batteries at high-rate cycling, coating of the nanorods by a protective layer has been proposed. The capacity of α-MoO_3-In_2O_3 core-shell nanorods maintains 1114 mAh g^{-1} and 443 mAh g^{-1} after 50 cycles at 0.2C and 2C rate, respectively [291]. Conformal passivation of the surface of MoO_3 nanorods by HfO_2 using atomic layer deposition (ALD) was proposed with success [292]. After 50 charge/discharge cycles at high current density1500 mA g^{-1}, HfO_2-coated MoO_3 electrodes exhibited a specific capacity of 657 mAh g^{-1}. MoO_3 nanoparticles were electrodeposited on Ti nanorod arrays that showed enhanced rate capability (300 mAh g^{-1} at 100 A g^{-1}) and excellent durability (retaining 300 mAh g^{-1} after 1500 cycles at 20 A g^{-1}) [293]. α-MoO_3/MWCNT nanocomposite delivered 490 mAh g^{-1} at current density 20 A g^{-1} owing to the high conductivity of the carbon nanotubes [294]. Porous MoO_3 grafted on TiO_2 nanotube array was found to improve the specific capacity with respect to MoO_3 alone and the TiO_2 nanotubes alone by a factor three [295]. A tremendous increase of capacity was achieved with SnO_2/MoO_3 core-shell nanobelts: 3104, 2214, 2172, 2110 and 2031 mAh g^{-1} at the 1st, 2nd, 10th, 20th and 30th, respectively, at C/10 rate. The reversible capacity after 50 cycles maintains 1895 mAh g^{-1} (C/10) and 1530 mAh g^{-1} (C/2) [296]. This result was explained by the fact that the Mo nanoparticles, generated together with Li_2O during the conversion reaction, increase the electrochemical reactivity and make the conversion between Li^+ and Li_2O reversible.

According to these results, MoO_3 shows good electrochemical properties for use as an anode for Li-ion batteries. The price to be paid to obtain such performance, however, is the reduction of the size of the particles to the nano-range, and the synthesis of nano-composites. Such synthesis processes, however, are not scalable, and expensive, which explains that the anode of the commercial Li-ion batteries is still graphitic carbon, although much better results are obtained since years at the laboratory scale, not only with MoO_3 but also with silicon and many metal oxides. In an attempt to make MoO_3 available as an anode for commercial Li-ion batteries, a facile scalable and not expensive method that improves the properties of the commercial MoO_3 was proposed [297]. The composite was formed of stoichiometric layered MoO_3, orthorhombic oxygen deficient phases $MoO_{3-\delta}$ with $\delta = 0.25$ (γ-Mo_4O_{11}) and α-$ZrMo_2O_8$. This $ZrMo_2O_8$-decorated composite delivered a capacity of 118 mAh g^{-1} at 2C rate, twice the capacity observed for the MoO_3 particles alone.

8.6. Iron Oxide-based Composites

Fe_2O_3 and Fe_3O_4 have drawn particular attention because of their high theoretical capacity of ≈1000 mAh g^{-1}, non-toxicity, and low processing cost. A recent review on the critical role of crystallite size, morphology, and electrode heterostructure of the pristine iron oxides on the

performance of the electrochemistry can be found in [298]. Again, the best results have been obtained in hybrid compounds.

8.6.1. Carbon-coated Iron Oxides

Carbon-coated Fe_3O_4 nanospindles delivered a capacity of 530 mAh g^{-1} after 80 charge/discharge cycles [299]. Better results have been obtained with carbon-coated Fe_3O_4 nanorods that delivered 808 mAh g^{-1} after 100 charge/discharge cycles at a current density of 924 mA g^{-1} [300]. In addition, the synthesis of the composite was made in a one-step process. 150–200 nm-thick Fe_3O_4 nanospheres coated with a thin layer of amorphous carbon with a uniform thickness of <6 nm forming a Fe_3O_4@C composite with specific surface area of <29 m^2 g^{-1} delivered a capacity of 712 mAh g^{-1} retained after 60 charge/discharge cycles at a current rate of 200 mAh g^{-1} [301].

Carbon-coated Fe_2O_3 hollow nanohorns on carbon nanotubes delivered a capacity of 820 mAh g^{-1} within 100 cycles at current density of 500 mA g^{-1} and the capacity retained at current density 3 A g^{-1} was still 400 mAh g^{-1} [302]. Other nano-composites with carbon nanofibers did not give better data [303]. The best result has been obtained recently with a mesoporous composite made of carbon-coated FeO_x particles (20 ± 14 nm-thick)/carbon nanotube (CNT) with high specific surface area (66 m^2 g^{-1}). As an anode, this composite delivered a specific capacity retention of 84% (445 mAh g^{-1}) after 2000 cycles at 2000 mA g^{-1} (4C) [304]. Note, however, that the amount of carbon was important, i.e. 43 wt%.

8.6.2. Iron Oxide-Carbon Nanosheets

In a different geometry, uniform-sized ferrite nanocrystals/carbon hybrid nanosheets as an anode maintained 600 mAh g^{-1} after 50 cycles where the cell was discharged with a constant current of 100 mA g^{-1} to 0.05 V (vs. Li^0/Li^+) and constant voltage at 0.05 V vs. Li^0/Li^+ to 50 mA g^{-1} and charged with a constant current of 100 mA g^{-1} to 3.0 V , and 81.5% of original capacity was retained after 5 cycles, where the lithiation and delithiation current density were fixed at 100 mA g^{-1} and 5 A g^{-1}, respectively [305]. A major improvement was achieved with a facile and scalable in situ synthesis of carbon-encapsulated Fe_3O_4 nanoparticles (<18.2 nm) homogeneously embedded in two-dimensional (2D) porous graphitic carbon nanosheets with a thickness of less than 30 nm. This composite as an anode delivered 858, 587, and 311 mAh g^{-1} at 5, 10, and 20C, respectively (1C = 1 A g^{-1}) and suffered only 3.47% capacity loss after 350 cycles at a high rate of 10C [306].

8.6.3. Iron Oxides-Graphene Composites

Two Fe_2O_3/graphene composites have been investigated [307,308]. The results are comparable. The capacity was 1027 mAh g^{-1} after 50 cycles at current density 100 mA g^{-1}. Recently, Fe_2O_3 nanoparticles encapsulated in g-C_3N_4/graphene (CN-G) sandwich-type nanosheets were synthesized. This Fe_2O_3/CN-G composite delivered 980 mAh g^{-1} after 50 cycles at a current density of 50 m g^{-1}, preserving 76.4% of the initial capacity. 532 mAh g^{-1} and 436 mAh g^{-1} after 100 cycles at current

densities of 1 and 2 A g^{-1}, respectively [309].

Fe_3O_4/graphene composites were also synthesized. Considering only the better results obtained in the recent years, we note free standing (i.e. binder less) hollow Fe_3O_4/graphene (39.6 wt% graphene) with hollow and porous Fe_3O_4 that delivered 1400 and 660 mAh g^{-1} after 50 cycles at current densities100 and 500 mA g^{-1}, respectively [310]. Another composite with 25 wt% graphene delivered a capacity of 826 mAh g^{-1} after 100 cycles at current density of 1 A g^{-1}. The capacity was still 460 mAh g^{-1} at 5 A g^{-1} [311]. The improved performance was attributed to a new method to obtain well-dispersed Fe_3O_4 particles uniformly with high loading.

8.6.4. Ternary Compounds

Ternary composites have been recently proposed. To compensate the lower capacity of TiO_2, the hierarchical co-assembly of TiO_2 nanorods and Fe_3O_4 nanoparticles on pristine graphene nanosheets has been proposed to address simultaneously the lower capacity of TiO_2 by coupling it with Fe_3O_4, and their low electrical conductivity by coupling them with graphene [312]. The TiO_2 nanorods/Fe_3O_4 nanoparticles/pristine graphene ternary heterostructures (40:20:40) delivered a reversible capacity up to 703 mAh g^{-1} at the end of 200 charging-discharging cycles at a current density of 500 mA g^{-1}, corresponding to 90% cycle retention, and 524 mAh g^{-1} after 200 cycles at 1 A g^{-1}. This performance is remarkable as it allies high capacity, especially at high rates, and high cycleability. The capacity is higher than the TiO_2/reduced-GO anode reported previously, e.g. 190 mAh g^{-1} at 320 mA g^{-1} [313], 161 mAh g^{-1} at 170 mA g^{-1} [314], 200 mAh g^{-1} at 100 mA g^{-1} [315] or 175 mAh g^{-1} at 100 mA g^{-1} [316]. This is attributed by the authors to the high-capacity Fe_3O_4 as an auxiliary active material, and also the choice of pristine graphene rather than reduced graphene oxide (r-GO), because the electronic properties of r-GO are damaged during the oxidation-reduction process needed to prepare it. The good cycleability is due to the fact that the fraction (20 wt%) of Fe_3O_4 is small, to take full advantage that the change of volume of TiO_2 during cycling is small, at contrast with the other active anode elements except $Li_4Ti_5O_{12}$, so that the resulting aging of the anode is reduced. For comparison, a TiO_2/Fe_2O_3 anode where the Fe_2O_3 fraction is up to 42.9 wt%, had reduced performance, namely 430.2 mAh g^{-1} at 200 mA g^{-1} after 100 cycles [317].

8.7. Co_3O_4-based Composites

According to the conversion reaction, the theoretical capacity of Co_3O_4 is 890 mAh g^{-1}. However, its electrical conductivity is very small. One possibility to overcome this difficulty is to dope this compound, and indeed, C-N co-doped Co_3O_4 hollow nanofibers gave promising performance as an anode [318]. Otherwise, the solution was to build nano-Co_3O_4/carbon composites. Recently, a Co_3O_4/porous carbon nanofibers composite delivered 869.5 mAh g^{-1} at 0.1C 94.9% capacity retention at 50 cycles at 0.1C-rate, and 403.6 mAh g^{-1} at 2C at 25 cycles [319]. The best results, however, were obtained with graphene.

Co_3O_4 nanoparticles in a size range of 2–3 nm confined in a few-layered porous graphene nanomesh framework (70% Co_3O_4) delivered 1543 mAh g^{-1} at 150 mA g^{-1} and 1075 mAh g^{-1} at

1000 mA g^{-1} [320]. Even at the high current density of 1000 mA g^{-1}, the capacity was still 1072 mAh g^{-1}, while that of previously reported Co_3O_4/graphene composites was in the range 500–600 mAh g^{-1} [321,322]. At low current density, the capacity is comparable to that of the CoO/graphene composite [249], but the decrease with the number of cycles is smaller in the Co_3O_4/graphene composite. Mesoporous Co_3O_4 nanosheets-3D graphene networks (specific surface area and pore size 34.5 m^2 g^{-1} and <3.8 nm, respectively) delivered 630 mAh g^{-1} after 50 cycles at 0.2C, and 130 mAh g^{-1} at 5C [323]. A well-dispersed Co_3O_4 nanoparticles with high density anchored on nitrogen-doped graphene (CNGs) delivered a reversible capacity of 867.9 mAh g^{-1} after 350 cycles at current density 50 mAh g^{-1} and exhibited a high rate capability (155.6 mAh g^{-1} at 2 A g^{-1} [324]. Recently, a mesoporous atomic layer-by-layer Co_3O_4 nanosheets/graphene mesoporous composite discharge capacities of 2014.7 and 1134.4 mAh g^{-1} at 0.11 and 2.25C, respectively, and capacity retention of 92.1% after 2000 cycles at 2.25C [325]. This outperforms all previous results. However, this synthesis process seems limited to the laboratory scale.

Composite composed of anatase TiO_2 nanofibers and secondary porous Co_3O_4 nanosheets have been prepared to take advantage of the high capacity of anatase TiO_2 (in the same way as in the TiO_2/Fe_3O_4 case already discussed in the section devoted to the iron oxides). This TiO_2/Co_3O_4 composite delivered 632.5 mAh g^{-1} and 95.3% capacity retention after 480 cycles, and 449.5 mAh g^{-1} at current density of 1 A g^{-1} [326].

9. Conclusion

Titanium oxides have the disadvantage of a lower energy density than that of graphite, typically 160 mAh g^{-1} for $Li_4Ti_5O_{12}$, 250 mAh g^{-1} for TiO_2 vs. 372 mAh g^{-1}. Also, the voltage at which Li cycling occurs in the titanium oxides is high, namely 1.3–1.6 V, which reduces the operating voltage of the Li-ion battery, and thus its energy density. On another hand, this potential has the advantage of avoiding the large irreversible capacity lost due to the formation of the SEI on anode particles operating below 1 V. The titanium oxides have other remarkable advantages: low cost, environmental safety, very good stability both in the discharged and charged state, very good cycleability and very high power density, very good abuse tolerance. That is why $Li_4Ti_5O_{12}$ is expected to be accepted for hybrid and different applications, in particular when high power density is needed, in particular under the form of carbon-coated $Li_4Ti_5O_{12}$. This composite anode has a remarkable rate capability. In addition, the nano-size of the structures that have been built during last years, increases the surface over volume ratio, and introduces additional active sites at the surface, so that the experimental reversible capacities can be larger than the theoretical one, solving the problem of the capacity retention.

Alloying materials such as Si, Ge, SiO, SnO_2 can provide much larger capacities, and energy densities than the titanium oxides and the other elements of the previous group, but they suffer from the important capacity loss upon cycling due to the large variation of volume upon Li insertion and de-insertion. Si and SnO_2 are the most promising elements of this family, as germanium is expensive and not abundant in nature. The same problem is met with oxide anodes based on conversion reactions. In addition, these anodes exhibit large potential hysteresis between the charge and discharge reactions. The voltage hysteresis, however, is expected to be solved by using some

catalysts and surface coating. Important improvements in the cycleability and rate capability of these anodes have been obtained in the last few years.

Both the alloying anode materials and the oxide anodes based on conversion reactions have benefited from the progress in the preparation of porous nanostructures by different processes involving thermal decomposition of hydroxide, carbonate, oxalate, etc., which are much more scalable than prior methods. Another progress at the laboratory scale has been the synthesis of composites, in particular with graphene. Graphene has a very good electronic conductivity, a good mechanical flexibility and high chemical functionality. Therefore, it can serve as an ideal 2D support for assembling nanoparticles with various structures and very good results have been obtained with composites graphene-nanoparticles of metal oxides. In addition the graphene is able to prevent agglomeration of the nanoparticles upon cycling, and the nanoparticles prevent the re-stacking of the graphene sheets. The development of metal oxides based on alloying or conversion reaction, in addition of titanium oxides based on the intercalation process we have reviewed can now be prepared under the form of nanoporous structure supported by graphene sheets, which are able to deliver a reversible capacity the order of 700 mAh g^{-1} for 1000 cycles at the laboratory scale.

The handicap for the development of such anodes is now the cost, and a scalable production of these nanostructured composites. This is a big challenge that hinders the mass production of such anodes until the problem has been solved. Also the composites carbon nanotubes-nanoparticles of metal oxides can be presently prepared only at the laboratory scale, as production cost and the low speed at which they can be synthesized does not permit their application in the battery industry. Hopefully, recent results suggest that the forcespinning technology is a viable method for the large scale production of nano/micro fibers for battery electrodes [327]. This technology has the capability for dual materials feed with an almost 100% yield and solvent-free processing for melt spinning.

The main efforts in the recent years have been to increase the performance of the anode materials. However, the capacity is limited more by the cathode than the anode element in Li-ion batteries: typically, the capacity of a cathode element is in the range 140–200 mAh g^{-1}. The gain in capacity of the total cell by increasing that of the anode element alone is thus limited, as the total capacity almost saturates when the anode capacity reaches typically 500 mAh g^{-1} [2]. Many composites today can deliver such a capacity and even much more for a thousand of cycles. Somehow, the run on the performance of anodes is over. Time is to focus on scalable synthesis of these composites at a reasonable price to supplement the graphite anodes.

Conflict of Interest

The authors declare that there is no conflict of interest regarding the publication of this manuscript.

References

1. Zaghib K, Mauger A, Julien CM (2015) Rechargeable lithium batteries for energy storage in smart grids, In: *Rechargeable Lithium Batteries*, Woodhead Publishing Series in Energy number 81, Elsevier.

2. Kasavajjula U, Wang C, Appleby AJ (2007) Nano- and bulk-silicon-based insertion anodes for lithium-ion secondary cells. *J Power Sources* 163: 1003–1039.
3. Julien CM, Mauger A, Vijh A, et al. (2016) Lithium Batteries: Science and Technology, Springer, New York, 323–429.
4. Zhao K, Pharr M, Hartle L, et al. (2012) Fracture and debonding in lithium-ion batteries with electrodes of hollow core-shell nanostructures. *J Power Sources* 218: 6–14.
5. Ma ZS, Xie ZC, Wang Y, et al. (2015) Failure modes of hollow core-shell structural active materials during the lithiation-delithiation process. *J Power Sources* 290: 114–122.
6. Wang C, Ma Z, Wang Y, et al. (2016) Failure prediction of high-capacity electrode materials in lithium-ion batteries. *J Electrochem Soc* 163: A1157–A1163.
7. Jiang W, Li T, Ma Z, et al. (2015) Optimal design of hollow core-shell structural active materials for lithium ion batteries. *Results in Phys* 5: 250–252.
8. Hu Y, Zhao X, Suo Z (2010) Averting cracks caused by insertion reaction in lithium-ion batteries. *J Mater Res* 25: 1007–1010.
9. Wang Y, Ma Z, Lei W, et al. (2016) Double effect of electrochemical reaction and substrate on hardness in electrodes of lithium-ion batteries. *Acta Mechan* 1–6.
10. Ma Z, Li T, Huang YL, et al. (2013) Critical silicon-anode size for averting lithiation-induced mechanical failure of lithium-ion batteries. *RSC Adv* 3: 7398–7402.
11. Haftbaradaran H, Gao H (2012) Ratcheting of silicon island electrodes on substrate due to cyclic intercalation. *Appl Phys Lett* 100: 121907.
12. Xie Z, Ma Z, Wang Y, et al. (2016) A kinetic model for diffusion and chemical reaction of silicon anode lithiation in lithium ion batteries. *RSC Adv* 6: 22383–22388.
13. Zhang P, Ma Z, Wang Y, et al. (2015) A first principles study of the mechanical properties of Li-Sn alloys. *RSC Adv* 5: 36022–36029.
14. Zhang P, Ma Z, Jiang W, et al. (2016) Mechanical properties of Li-Sn alloys for Li-ion battery anodes: A first-principles perspective. *AIP Adv* 6: 015107.
15. Gao X, Ma Z, Jiang W, et al. (2016) Stress-strain relationships of Li_xSn alloys for lithium ion batteries. *J Power Sources* 311: 21–28.
16. Sony press news (2005) Available from: www.Sony.net/SonyInfo/News/Press/200502/05-006E/index.html.
17. Agubra VA, Zuniga L, Flores D, et al. (2016) Composite nano-fibers as advanced materials for Li-ion, Li-O_2 and Li-S batteries. *Electrochim Acta* 192: 529–550.
18. Aravindan V, Sundaramurthy J, Kumar PS, et al. (2015) Electrospun nanofibers: A prospective electro-active material for constructing high performance Li-ion batteries. *Chem Commun* 51: 2225–2234.
19. Jung JW, Lee CL, Yu S, et al. (2016) Electrospun nanofibers as a platform for advanced secondary batteries: a comprehensive review. *J Mater Chem A* 4: 703–750.
20. Goodenough JB, KimY (2010) Challenges for rechargeable Li batteries. *Chem Mater* 22: 587–603.
21. Liu Y, Yang Y (2016) Recent progress of TiO_2-based anodes for Li ion batteries. *J Nanomater* 2016: 1–15.
22. Zhang Y, Tang Y, Li W, et al. (2016) Nanostructured TiO_2-based anode materials for

high-performance rechargeable lithium-ion batteries. *ChemNanoMat*.
23. Rahman A, Wong Y, Song G, et al. (2015) A review on porous negative electrodes for high performance lithium-ion batteries. *J Porous Mater* 22: 1313–1343.
24. Niu J, Zhang S, Niu Y, et al. (2015) Silicon-based anode materials for lithium-ion batteries. *Prog Chem* 27: 1275–1290.
25. Roy P, Srivastava K (2015) Nanostructured anode materials for lithium ion batteries. *J Mater Chem A* 3: 2454–2484.
26. Ji L, Lin Z, Alcoutlabi M, et al. (2011) Recent developments in nanostructured anode materials for rechargeable lithium-ion batteries. *Energy Environ Sci* 4: 22682–2699.
27. Zhang WJ (2011) A Review of the electrochemical performance of alloy anodes for lithium-ion batteries. *J Power Sources* 196: 13–24.
28. Lou S, Cheng X, Ma Y, et al. (2015) Nb-based oxides as anode materials for lithium ion batteries. *Prog Chem* 27: 297–309.
29. Lahiri I, Oh SM, Hwang JY, et al. (2011) Ultrathin alumina-coated carbon nanotubes as an anode for high-capacity Li-ion batteries. *J Mater Chem* 21: 13621–13626.
30. Leung K, Qi Y, Zavadil KR, et al. (2011) Using atomic layer deposition to hinder solvent decomposition in lithium-ion batteries: first principles modeling and experimental studies. *J Am Chem Soc* 133: 14741–14754.
31. De Las Cazas C, Li WZ (2012) A review of application of carbon nanotubes for lithium-ion battery anode material. *J Power Sources* 208: 74–85.
32. Fan S, Sun T, Rui X, et al. (2012) Cooperative enhancement of capacities in nanostructured SnSb/carbon nanotube network nanocomposite as anode for lithium ion batteries. *J Power Sources* 201: 288–293.
33. Wu Y, Wei Y, Wang J, et al. (2013) Conformal Fe_3O_4 sheath on aligned carbon nanotube scaffolds as high-performance anodes for lithium-ion batteries. *Nano Lett* 13: 818–823.
34. Ban C, Wu Z, Gillaspie DT, et al. (2010) Nanostructured Fe_3O_4/SWNT electrode: binder-free and high-rate Li-ion anode. *Adv Energy Mater* 22: E145–E149.
35. Bindumadhavan K, Srivastava SK, Mahanty S (2013) MoS_2-MWCNT hybrids as a superior anode in lithium-ion batteries. *Chem Commun* 49: 1823–1825.
36. Wang ZL, Xu D, Wang HG, et al. (2013) In-situ fabrication of porous graphene electrodes for high performance energy storage. *ACS Nano* 7: 2422–2430.
37. Lavoie N, Courtel F, Malenfant PRL, et al. (2013) Graphene-based composite anodes for lithium-ion batteries, In: *Nanotechnology for Lithium-Ion Batteries*, ed. by Y. Abdu-Lebdeh, I. Davidson, Springer, New York.
38. Fu YS, Zhu JW, Hu C, et al. (2014) Covalently coupled hybrid of graphitic carbon nitride with reduced graphene oxide as a superior performance lithium-ion battery anode. *Nanoscale* 6: 12555–12564.
39. Takamura T, Ohara S, Uehara M, et al. (2004) A vacuum deposited Si film having a Li extraction capacity over 2000 mAh g^{-1} with a long cycle life. *J Power Sources* 129: 96–100.
40. Ohara S, Suzuki J, Sekine K, et al. (2003) Li insertion/extraction reaction at a Si film evaporated on a Ni foil. *J Power Sources* 119–121: 591–596.
41. Chen LB, Xie JY, Yu HC, et al. (2009) An amorphous thin film Si anode with high capacity and

long cycling life for lithium ion batteries. *J Appl Electrochem* 39: 1157–1162.
42. Ohara S, Suzuki J, Sekine K, et al. (2004) A thin film silicon anode for Li-ion batteries having a very large specific capacity and long cycle life. *J Power Sources* 136: 303–306.
43. Kim JB, Lee, HY, Lee KS, et al. (2003) Fe/Si multi-layer thin film anodes for lithium rechargeable thin film batteries. *Electrochem Commun* 5: 544–548.
44. Lee HY, Lee SM (2002) Graphite-FeSi alloy composites as anode materials for rechargeable lithium ion batteries. *J Power Sources* 112: 649–654.
45. Yu C, Li X, Ma T, et al. (2012) Silicon thin films as anodes for high-performance lithium-ion batteries with effective stress relaxation. *Adv Energy Mater* 2: 68–73.
46. Liu Y, Hudak NS, Huber DL, et al. (2011) In-situ transmission electron microscopy observation of pulverization of aluminum nanowires and evolution of the thin surface Al_2O_3 layers during lithiation-delithiation cycles. *Nano Lett* 11: 4188–4194.
47. Xiao X, Lu P, Dahn J (2011) Ultrathin multifunctional oxide coatings for lithium ion batteries. *Adv Mater* 23: 3911–3915.
48. He Y, Yu X, Wang Y, et al. (2011) Alumina-coated patterned amorphous silicon as the anode for a lithium ion battery with high coulombic efficiency. *Adv Mater* 23: 4938–4941.
49. Ge M, Rong J, Fang X, et al. (2012) Porous doped silicon nanowires for lithium ion battery anode with long cycle life. *Nano Lett* 12: 2318–2323.
50. Kim H, Cho J (2008) Superior lithium electroactive mesoporous Si@carbon core-shell nanowires for lithium battery anode material. *Nano Lett* 8: 3688–3691.
51. Lytle JC (2013) Inverse opal nanoarchitecture as lithium ion anode materials. In: *Nanotechnology for Lithium-Ion Batteries*, ed. by Y. Abdu-Lebdeh, I. Davidson, Springer, New York.
52. Chen HX, Dong ZX, Fu YP, et al. (2010) Silicon nanowires with and without carbon coating as anode materials for lithium ion batteries. *J Solid State Electrochem* 14: 1829–1834.
53. Sethuraman VA, Kowolik K, Sirinavan V (2011) Increased cycling efficiency and rate capability of copper-coated silicon anode materials for lithium-ion batteries. *J Power Sources* 196: 6657–6662.
54. Yao Y, Liu N, McDowell MT, et al. (2012) Improving the cycling stability of silicon nanowire anodes with conducting polymer coatings. *Energy Environ Sci* 5: 7927–7930.
55. Memarzadeh EL, Kalisvaart WP, Kohandehghan A, et al. (2012) Silicon nanowire core aluminium shell coaxial nanocomposites for lithium ion anodes grown with and without a TiN interlayer. *J Mater Chem* 22: 6655–6668.
56. Ruy I, Choi JW, Cui Y, et al. (2011) Size dependent fracture of Si nanowire battery anodes. *J Mechan Phys Solids* 59: 1717–1730.
57. Liu XH, Zheng H, Zhong L, et al. (2011) Anisotropic swelling and fracture of silicon nanowires during lithiation. *Nano Lett* 11: 3312–3318.
58. Nguyen HT, Zamfir MR, Duong LD, et al. (2012) Alumina-coated silicon-based nanowire arrays for high quality Li-ion battery anodes. *J Mater Chem* 22: 24618–24626.
59. Wu H, Chan G, Choi JW, et al. (2012) Stable cycling for double-walled silicon nanotubes battery anodes through solid-electrolyte interphase control. *Nano Technol* 7: 310–315.
60. Song T, Cheng HY, Choi H, et al. (2012) Si/Ge double-layered nanotube array as a lithium ion

battery anode. *ACS Nano* 6: 303–309.
61. Rong J, Fang X, Ge M, et al. (2013) Coaxial Si/anodic titanium oxide/Si nanotube arrays for lithium-ion battery anodes. *Nano Res* 6: 182–190.
62. Choi NS, Yao Y, Cui Y, et al. (2011) One-dimensional Si/Sn-based nanowires and nanotubes for lithium-ion energy storage materials. *J Mater Chem* 21:9 825–9840.
63. Evanoff K, Kahn J, Balandin AA, et al. (2012) Towards ultra-thick battery electrodes: aligned carbon nanotube, enabled architecture. *Adv Mater* 24: 533–537.
64. Krishnan R, Lu TM, Koratkar N (2011) Functionally strain-graded nanoscoops for High Power Li-Ion Battery Anodes. *Nano Lett* 11: 377–384.
65. Kim H, Han B, Choo J, et al. (2008) Three-dimensional porous silicon particles for uses in high-performance lithium secondary batteries. *Angew Chem* 47: 10151–10154.
66. Son IH, Park JH, Kwon S, et al. (2015) Silicon carbide-free graphene growth on silicon for lithium-ion battery with high volumetric energy density. *Nature Commun* 6: 7393.
67. Wu H, Zheng G, Liu N, et al. (2012) Engineering empty space between Si nanoparticles for lithium-ion battery anodes. *Nano Lett* 12: 904–909.
68. Liu N, Wu H, McDowell MT, et al. (2012) A yolk-shell design for stabilized and scalable li-ion battery alloy anodes. *Nano Lett* 12: 3315–3325.
69. Liu N, Lu Z, Zhao J, et al. (2014) A pomegranate-inspired nanoscale design for large-volume-change lithium battery anodes. *Nat Nanotechnol* 9: 187–190.
70. Chou SL, Wang JZ, Choucair M, et al. (2010) Enhanced reversible lithium storage in a nanosize silicon/graphene composite. *Electrochem Commun* 12: 303–306.
71. Wang JZ, Zhong C, Chou SL, et al. (2010) Flexible free-standing graphene-silicon composite film for lithium-ion batteries. *Electrochem Commun* 12: 1467–1470.
72. Lee JK, Smith KB, Hayner CM, et al. (2010) Silicon nanoparticles-graphene paper composites for Li ion battery anodes. *Chem Commun* 46: 2025–2027.
73. Chen S, Bao P, Huang X, et al. (2014) Hierarchical 3D mesoporous silicon@graphene nanoarchitectures for lithium ion batteries with superior performance. *Nano Res* 7: 85–94.
74. Zhao X, Hayner CM, Kung MC, et al. (2011) In-plane vacancy-enabled high-power Si-graphene composite electrode for lithium-ion batteries. *Adv Energy Mater* 1: 1079–1084.
75. Zhao X, Li M, Chang KH, et al. (2014) Composites of graphene and encapsulated silicon for practically viable high-performance lithium-ion batteries. *Nano Res* 7: 1429–1438.
76. Zamfir MR, Nguyen HT, Moyen E, et al. (2013) Silicon nanowires for Li-based battery anodes: a review. *J Mat Chem A* 1: 9566–9586.
77. Wen Z, Lu G, Mao S, et al. (2013) Silicon nanotube anode for lithium-ion batteries. *Electrochem Commun* 29: 67–70.
78. Baggetto L, Notten PHN (2009) Lithium ion (de)insertion reaction of germanium thin-film electrodes and electrochemical and in-situ XRD study batteries and energy storage. *J Electrochem Soc* 156: A169–A175.
79. Liu XH, Huang S, Picraux ST, et al. (2011) Reversible nanopore formation in Ge nanowires during lithiation-delithiation cycling: an in-situ transmission electron microscopy study. *Nano Lett* 11: 3991–3997.
80. Liang W, Yang H, Fan F, et al. (2013) Tough germanium nanoparticles under electrochemical

cycling. *ACS Nano* 7: 3427–3433.
81. Graetz J, Ahn CC, Yazami R, et al. (2004) Nano crystalline and thin film germanium electrodes with high lithium capacity and high rate capabilities. *J Electrochem Soc* 151: A698–A702
82. Ren JG, Wu Q-H, Tang H, et al. (2013) Germanium-graphene composite anode for high-energy lithium batteries with long cycle life. *J Mater Chem A* 1: 1821–1826.
83. Fang S, Shan L, Zheng H, et al. (2015) Ge-graphene-carbon nanotube composite anode for high performance lithium-ion batteries. *J Mater Chem A* 3: 1498–1503.
84. DiLeo RA, Frisco S, Ganter MJ, et al. (2011) Hybris germanium nanoparticle—single wall carbon nanotube free-standing anodes for lithium batteries. *J Phys Chem C* 115: 22609–22614.
85. Ashuri M, He Q, Shaw LL (2016) Silicon as a potential anode material for Li-ion batteries: where size, geometry and structure matter. *Nanoscale* 8: 74–103.
86. Kamali AR, Fray DJ (2011) Tin-based as advanced anode materials for lithium-ion batteries: a review. *Rev Adv Mater Sci* 27: 14–24.
87. Youn DH, Heller A, Mullins CB (2016) Simple synthesis of nanostructured Sn/nitrogen-doped carbon composite using nitrilotriacetic acid as lithium ion Battery Anode. *Chem Mater* 28: 1343–1347.
88. Yu Y, Gu L, Wang C, et al. (2009) Encapsulation of Sn-carbon nanoparticles in bamboo-like hollow carbon nanofibers as an anode material in lithium-based batteries. *Angew Chem Int Ed* 48: 6485–6489.
89. Wang Y, Ma Z, Lu C (2016) A twins-structural Sn@C core-shell composite as anode materials for lithium-ion batteries. *Compos Interface* 23: 273–280.
90. Liang S, Zhu X, Lian P, et al. (2011) Superior cycle performance of Sn@C/graphene nanocomposite as an anode material for lithium-ion batteries. *J Solid Stat Chem* 184: 1400–1404.
91. Agubra VA, Zuniga L, De La Garza D, et al. (2016) Forcespinning: A new method for the mass production of Sn/C composite nano fiber anodes for lithium ion batteries. *Solid State Ionics* 286: 72–82.
92. Beaulieu LY, Dahn JR (2000) The reaction of lithium with Sn-Mn-C intermetallics prepared by mechanical alloying. *J Electrochem Soc* 147: 3237–3241.
93. Mao O, Dunlap RA, Dahn JR (1999) Mechanically alloyed Sn-Fe-C powders as anode materials for Li-ion batteries. I. The Sn_2Fe-C system. *J Electrochem Soc* 146: 405–413.
94. Mao O, Dahn JR (1999) Mechanically alloyed Sn-Fe-C powders as anode materials for Li-ion batteries. II. The Sn-Fe system. *J Electrochem Soc* 146: 414–422.
95. Mao O, Dahn J (1999) Mechanically alloyed Sn-Fe-C powders as anode materials for Li-ion batteries. III. Sn_2Fe: $SnFe_3C$ active/inactive composites. *J Electrochem Soc* 146: 423–427.
96. Dahn JR, Mar RE, Abouzeid A (2006) Combinatorial study of $Sn_{1-x}Co_x$ ($0 < x < 0.6$) and $[Sn_{0.55}Co_{0.45}]_{1-y}C_y$ ($0 < y < 0.5$) alloy negative electrode materials for Li-ion batteries. *J Electrochem Soc* 153: A361–A365.
97. Hassoun J, Ochal P, Panero S, et al. (2008) The effect of $CoSn/CoSn_2$ phase ratio on the electrochemical behavior of $Sn_{40}Co_{40}C_{20}$ ternary alloy electrodes in Li cells. *J Power Sources* 180: 568–575.
98. Hassoun J, Mulas G, Panero S, et al. (2007) Ternary Sn-Co-C Li-ion battery electrode material

prepared by high energy ball milling. *Electrochem Commun* 9: 2075–2081.
99. Mukaibo H, Sumi T, Yokoshima T, et al. (2003) Electrodeposited Sn-Ni alloy film as a high capacity anode material for lithium-ion secondary batteries. *Electrochem Solid-State Lett* 6: A218–A220.
100. Wolfenstine J, Campos S, Foster D, et al. (2002) Nano-scale Cu_6Sn_5 anodes. *J Power Sources* 109: 230–233.
101. Ferguson PP, Todd ADW, Dahn JR (2008) Comparison of mechanically alloyed and suttered tin-cobalt-carbon as an anode material for lithium-ion batteries. *Electrochem Commun* 10: 25–31.
102. Hassoun J, Panero S, Mulas G, et al. (2007) An electrochemical investigation of a Sn-Co-C ternary alloy as a negative electrode in Li-ion batteries. *J Power Sources* 171: 928–931.
103. Sony corporation (2011) Sony the market for notebook PC; development of a tin-based amorphous anode for high-capacity rechargeable lithium-ion battery 3.5 Ah: the "Nexelion". Available from: http:www.sony.co.jp/SonyInfo/News/Press/201107/11-078/.
104. Lei WX, Pan Y, Zhou YC, et al. (2014) CNTs-Cu composite layer enhanced Sn-Cu alloy as high performance anode materials for lithium-ion batteries. *RSC Adv* 4: 3233–3237.
105. Meschini I, Nobili F, Mancini M, et al. (2013) High performance Sn@carbon nanocomposite anode for lithium batteries. *J Power Sources* 226: 241–248.
106. Jiang W, Zeng W, Ma Z, et al. (2014) Advanced amorphous nanoporous stannous oxide composite with carbon nanotubes as anode materials for lithium-ion batteries. *RSC Adv* 4: 41281–41286.
107. Zhu XJ, Guo ZP, Zhang P, et al. (2009) Highly porous reticular tin-cobalt oxide composite thin film anodes for lithium ion batteries. *J Mater Chem* 19: 8360–8365.
108. Zhu XJ, Guo ZP, Zhang P, et al. (2010) Three-dimensional reticulartin-manganese oxide composite anode materials for lithium ion batteries. *Electrochim Acta* 55: 4982–4986.
109. Chen JS, Cheah YL, Chen YT, et al. (2009) SnO_2 nanoparticles with controlled nano-coating as high-capacity anode for lithium-ion batteries. *J Phys Chem* 113: 20504–20508.
110. He M, Yuan L, Zhang W, et al. (2013) A SnO_2-carbon nanocluster anode material with superior cyclablity and rate capability for lithium batteries. *Nanoscale* 5: 3298–3305.
111. Hassan MF, Rahman MM, Guo Z, et al. (2010) SnO_2-NiO-C nanocomposite as a high capacity anode material for lithium-ion batteries. *J Mater Chem* 20: 9707–9712.
112. Yesibolati N, Shahid M, Chen W, et al. (2014) SnO_2 anode surface passivation by atomic layer deposited HfO_2 improves Li-ion battery performance. *Small* 10: 2849–2858.
113. Du Z, Zhang S, Jiang T, et al. (2012) Facile synthesis of SnO_2 nanocrystals coated conductive polymer nanowires for enhanced lithium storage. *J Power Sources* 219: 199–203.
114. Lou XW, Li CM, Archer LA (2009) Design synthesis of coaxial SnO_2@carbon hollow nanospheres for highly reversible lithium storage. *Adv Mater* 21: 2536–2539.
115. Wang Z, Fierke MA, Stein A (2008) Porous carbon/tin oxide monoliths as anodes for lithium-ion batteries. *J Electrochem Soc* 155: A658–A663.
116. Zhang L, Wu HB, Liu B, et al. (2014) Formation of porous SnO_2 microboxes via selective leaching for highly reversible lithium storage. *Energy Environ Sci* 7: 1013–1017.
117. Du G, Zhong C, Zhang P, et al. (2010) Tin dioxyde/carbon nanotube composites with high

uniform SnO_2 loading as anode materials for lithium ion batteries. *Electrochim Acta* 55: 2582–2586.
118. Ren JR, Yang J, Abouimrane A, et al. (2011) SnO_2 nanocrystals deposited on multiwalled carbon nanotubes with superior stability as anode material for Li-ion batteries. *J Power Sources* 196: 8701–8705.
119. Zhu CL, Zhang ML, Qiao YJ, et al. (2010) High capacity and good cycling stability of multi-walled carbon nanotube/SnO_2 core-shell structures as anode materials of lithium-ion batteries. *Mater Res Bull* 45: 437–441.
120. Wang Y, Zeng HC, Lee JY (2006) Highly reversible lithium storage in porous SnO_2 nanotubes with coaxially grown carbon nanotubes overlayers. *Adv Mater* 18: 645–649.
121. Zhang J, Ma Z, Jiang W, et al. (2016) Sandwich-like CNTs@SnO_2/SnO/Sn anodes on three-dimensional Ni foam substrate for lithium ion batteries. *J Electroanal Chem* 767: 49–55.
122. Li YM, Lv XJ, Lu J, et al. (2010) Preparation of SnO_2-nanocrystal/graphene-nanosheets composites and their lithium storage ability. *J Phys Chem C* 114: 21770–21774.
123. Zhao B, Zhang GH, Song JS, et al. (2011) Bivalent tin ion assisted reduction for preparing graphene/SnO_2 composite with good cyclic performance and lithium storage capacity. *Electrochim Acta* 56: 7340–7346.
124. Zhong C, Wang JZ, Chen ZX, et al. (2011) Photoinduced optical transparency in dye-sensitized solar cells containing graphene nanoribbons. *J Phys Chem C* 115: 25115–25131.
125. Lian PC, Zhu XF, Liang SZ, et al. (2011) High reversible capacity of SnO_2/graphene nanocomposite as an anode material for lithium-ion batteries. *Electrochim Acta* 56: 4532–4539.
126. Huang XD, Zhou XF, Zhou LA, et al. (2011) A facile one-step solvothermal synthesis of SnO_2/graphene nanocomposite and its application as an anode material for lithium-ion batteries. *ChemPhysChem* 12: 278–281.
127. Xie J, Liu SY, Chen XF, et al. (2011) Nanocrystal-SnO_2-loaded graphene with improved Li-storage properties prepared by a facile one-pot hydrothermal route. *Int J Electrochem Sci* 6: 5539–5549.
128. Baek S, Yu SH, Park SK, et al. (2011) A one-pot microwave-assisted non-aqueous sol-gel approach to metal oxide/graphene nanocomposites for Li-ion batteries. *RSC Adv* 1: 1687–1690.
129. Wang XY, Zhou XF, Yao K, et al. (2011) A SnO_2/graphene composite as a high stability electrode for lithium ion batteries. *Carbon* 49: 133–139.
130. Xu CH, Sun J, Gao L (2012) Direct growth of monodisperse SnO_2 nanorods on graphene as high capacity anode materials for lithium ion batteries. *J Mater Chem* 22: 975–979.
131. Lin J, Peng Z, Xiang C, et al. (2013) Graphene nanoribbon and nanostructured SnO_2 composite anodes for lithium ion batteries. *ACS Nano* 7: 6001–6007.
132. Zhou X, Wan LJ, Guo YG (2013) Binding SnO_2 nanocrystals in nitrogen-doped graphene sheets as anode materials for lithium-ion batteries. *Adv Mater* 25: 2152–2157.
133. Botas C, Carriazo D, Singh G, et al. (2015) Sn- and SnO_2-graphene flexible foams suitable as binder-free anodes for lithium ion batteries. *J Mater Chem A* 25: 13402–13410.
134. Jiang W, Zhao X, Ma Z, et al. (2016) SnO_2/reduced graphene oxide nanocomposite as anode material for lithium-ion batteries with enhanced cyclability. *J Nanosci Nanotech* 16: 4136–4140.
135. Sun J, Xiao L, Jiang S, et al. (2015) Fluorine-doped SnO_2@graphene porous composite for high

capacity lithium-ion batteries. *Chem Mater* 27: 4594–4603.
136. Liu L, An M, Yang P, et al. (2015) Superior cycle performance and high reversible capacity of SnO_2/graphene composite as an anode material for lithium-ion batteries. *Sci Rep* 5: 9055.
137. Deng Y, Fang C, Chen G (2016) The developments of SnO_2/graphene nanocomposites as anode materials for high performance lithium ion batteries: a review. *J Power Sources* 304: 81–101.
138. Liu S, Wang R, Liu M, et al. (2014) Fe_2O_3-SnO_2 nanoparticle decorated graphene flexible films as high-performance anode materials for lithium-ion batteries. *J Mater Chem A* 2: 4598–4604.
139. Bhaskar A, Deepa M, Ramakrishna M, et al. (2014) Poly(3,4-ethylenedioxythiophene) sheath over a SnO_2 hollow spheres/graphene oxide hybrid for a durable anode in Li-ion batteries. *J Phys Chem C* 118: 7296–7306.
140. Ren H, Yu RB, Wang JY, et al. (2014) Multishelled TiO_2 hollow microspheres as anodes with superior reversible capacity for lithium ion batteries. *Nano Lett* 14: 6679–6684.
141. Wang HY, Chen JZ, Hy S, et al. (2014) High-surface-area mesoporous TiO_2 microspheres *via* one-step nanoparticle self-assembly for enhanced lithium-ion storage. *Nanoscale* 6: 14926–14931.
142. Xia T, Zhang W, Wang Z, et al. (2014) Amorphous carbon-coated TiO_2 nanocrystals for improved lithium-ion battery and photocatalytic performance. *Nano Energy* 6: 109–118.
143. Acevedo-Peña P, Haro M, Rincón ME, et al. (2014) Facile kinetics of Li-ion intake causes superior rate capability in multiwalled carbon nanotube@TiO_2 nanocomposite battery anodes. *J Power Sources* 268: 397–403.
144. Jiang X, Yang X, Zhu Y, et al. (2014) 3D nitrogen-doped graphene foams embedded with ultrafine TiO_2 nanoparticles for high-performance lithium-ion batteries. *J Mater Chem A* 2: 11124–11133.
145. Fu Y, Ming H, Zhou Q, et al. (2014) Nitrogen-doped carbon coating inside porous TiO_2 using small nitrogen-containing molecules for improving performance of lithium-ion batteries. *Electrochim Acta* 134: 478–485.
146. Chen WN, Jiang H, Hu YJ, et al. (2014) Mesoporous single crystals $Li_4Ti_5O_{12}$ grown on rGO as high-rate anode materials for lithium-ion batteries. *Chem Commun* 50: 8856–8859.
147. Xin X, Zhou XF, Wu JH, et al. (2012) Scalable synthesis of TiO_2/graphene nanostructured composite with high-rate performance for lithium ion batteries. *ACS Nano* 6: 11035–11043.
148. Mo RW, Lei ZY, Sun KN, et al. (2014) Facile synthesis of anatase TiO_2 quantum-dot/graphene-nanosheet composites with enhanced electrochemical performance for lithium-ion batteries. *Adv Mater* 26: 2084–2088.
149. Wang J, Zhou Y, Xiong B, et al. (2013) Fast lithium-ion insertion of TiO_2 nanotube and graphene composites. *Electrochim Acta* 88: 847–857.
150. Zhang X, Zhang J, Liu Y, et al. (2015) Improving the anode performances of TiO_2-carbon-rGO composites in lithium ion batteries by UV irradiation. *New J Chem* 39: 9345–9350.
151. Zha CY, He DF, Zou JW, et al. (2014) A minky-dot-fabric-shaped composite of porous TiO_2 microsphere/reduced graphene oxide for lithium ion batteries. *J Mater Chem A* 2: 16931–16938.
152. Fang Y, Lv Y, Che R, et al. (2013) Two-dimensional mesoporous carbon nanosheets and their derived graphene nanosheets: synthesis and efficient lithium ion storage. *J Am Chem Soc* 135: 1524–1530.

153. Lan T, Kiu H, Xie F, et al. (2015) Rutile TiO_2 mesocrystals/reduced graphene oxide with high-rate and long-term performance for lithium-ion batteries. *Sci Rep* 5: 8498.
154. Liu H, Bi Z, Sun XG, et al. (2011) Mesoporous TiO_2-B microspheres with superior rate performance for lithium ion batteries. *Adv Mater* 23: 3450–3454.
155. Yang Z, Du G, Guo Z, et al. (2011) TiO_2(B)-carbon composite nanowires as anode for lithium ion batteries with enhanced reversible capacity and cyclic performance. *J Mater Chem* 21: 8591–8596.
156. Yan X, Li Y, Li M, et al. (2015) Ultrafast lithium storage in TiO_2-bronze nanowires/N-doped graphene nanocomposites. *J Mater Chem A* 3: 4180–4187.
157. Etacheri V, Yourey JE, Bartlett BM (2014) Chemically bonded TiO_2-Bronze nanosheet/reduced graphene oxide hybrid for high-power lithium ion batteries. *ACS Nano* 8: 1491–1499.
158. Li MS, Li XF, Li WH, et al. (2015) Atomic layer deposition derived amorphous TiO_2 thin film decorating graphene nanosheets with superior rate capability. *Electrochem Commun* 57: 43–47.
159. Luo J, Xia X, Luo Y, et al. (2013) Rationally designed hierarchical TiO_2/Fe_2O_3 hollow nanostructures for improved lithium ion storage. *Adv Energy Mater* 3: 737–743.
160. Liao JY, Higgins D, Lui G, et al. (2013) Multifunctional TiO_2-C/MnO_2 core-double-shell nanowire arrays as high-performance 3D electrodes for lithium ion batteries. *Nano Lett* 13: 5467–5473.
161. Jeun JH, Park KY, Kim DH, et al. (2013) SnO_2@TiO_2 double-shell nanotubes for a lithium ion battery anode with excellent high rate cyclability. *Nanoscale* 5: 8480–8483.
162. Jung HG, Myung ST, Yoon CS, et al. (2011) Microscale spherical carbon-coated $Li_4Ti_5O_{12}$ as ultra high power anode material for lithium batteries. *Energy Environ Sci* 4: 1345–1351.
163. Zaghib K, Dontigny M, Guerfi A, et al. (2012) An improved high-power battery with increased thermal operating range: C-$LiFePO_4$/C-$Li_4Ti_5O_{12}$. *J Power Sources* 216: 192–200.
164. Li B, Han C, He YB, et al. (2012) Facile synthesis of $Li_4Ti_5O_{12}$/C composite with super rate performance. *Energy Environ Sci* 5: 9595–9602.
165. Zhao L, Hu YS, Li H, et al. (2011) Porous $Li_4Ti_5O_{12}$ coated with N-doped carbon from ionic liquids for Li-ion batteries. *Adv Mater* 23: 1385–1388.
166. Fan L, Tan X, Yu T, et al. (2016) $Li_4Ti_5O_{12}$/hollow graphitized nano-carbon composites as anode materials for lithium ion battery. *RCS Adv* 6: 26406–26411.
167. Shen L, Yuan C, Luo H, et al. (2011) Novel template-free solvothermal synthesis of mesoporous $Li_4Ti_5O_{12}$-C microspheres for high power lithium ion batteries. *J Mater Chem* 21: 14414–14416.
168. Lin C, Fan X, Yin Y, et al. (2014) Mono-dispersed mesoporous $Li_4Ti_5O_{12}$ submicrospheres as anode materials for lithium-ion batteries: morphology and electrochemical performances. *Nanoscale* 21: 6651–6650.
169. Jhan YR, Duh JG (2012) Synthesis of entanglement structure in nanosized $Li_4Ti_5O_{12}$/multi-walled carbon nanotubes composite anode material for Li-ion batteries by ball-milling-assisted solid-state reaction. *J Power Sources* 198: 294–297.
170. Shi Y, Wen L, Li F, et al. (2011) Nanosized $Li_4Ti_5O_{12}$/graphene hybrid materials with low polarization for high rate lithium ion batteries. *J Power Sources* 196: 8610–8617.
171. Li X, Qu M, Huai Y, et al. (2010) Preparation and electrochemical performance of $Li_4Ti_5O_{12}$/carbon/carbon nanotubes for lithium ion battery. *Electrochim Acta* 55: 2978–2982.

172. Jhan YR, Duh JG (2012) Synthesis of entanglement structure in nanosized $Li_4Ti_5O_{12}$/multi-walled carbon nanotubes composite anode material for Li-ion batteries by ball-milling-assisted solid-state reaction. *J Power Sources* 198: 294–297.
173. Ni H, Fan LZ (2012) Nano-$Li_4Ti_5O_{12}$ anchored on carbon nanotubes by liquid phase deposition as anode material for high rate lithium-ion batteries. *J Power Sources* 214: 195–199.
174. Shen L, Yuan C, Luo H, et al. (2012) In situ growth of $Li_4Ti_5O_{12}$ on multi-walled carbon nanotubes: novel coaxial nanocables for high rate lithium ion batteries. *J Mater Chem* 21: 761–767.
175. Zhu N, Liu W, Xue MQ, et al. (2010) Graphene as a conductive additive to enhance the high-rate capabilities of electrospun $Li_4Ti_5O_{12}$ for lithium-ion batteries. *Electrochim Acta* 55: 5813–5818.
176. Ge H, Hao T, Osgood H, et al. (2016) Advanced mesoporous spinel $Li_4Ti_5O_{12}$/rGO composites with increased surface lithium storage capability for high-power lithium-ion batteries. *ACS Appl Mater Inter* 8: 9162–9169.
177. Chen C, Agrawal R, Wang C (2015) High performance $Li_4Ti_5O_{12}$/Si composite anodes for Li-ion batteries. *Nanomaterials* 5: 1469–1480.
178. Li N, Mei T, Zhu Y, et al. (2012) Hydrothermal synthesis of layered $Li_{1.81}H_{0.19}Ti_2O_5{\cdot}xH_2O$ nanosheets and their transformation to single-crystalline $Li_4Ti_5O_{12}$ nanosheets as the anode materials for Li-ion batteries. *CrystEngComm* 14: 6435–6440.
179. Liu GY, Wang HY, Liu GQ, et al. (2013) Synthesis and electrochemical performance of high-rate dual-phase $Li_4Ti_5O_{12}$-TiO_2 nanocrystallines for Li-ion batteries. *Electrochim Acta* 87: 218–223.
180. Xu C, Xue L, Zhang W, et al. (2014) Hydrothermal synthesis of $Li_4Ti_5O_{12}$/TiO_2 nano-composite as high performance anode material for Li-ion batteries. *Electrochim Acta* 147: 506–512.
181. Zhong H, Yang G, Song H, et al. (2012) Vertically aligned graphene-like SnS_2 ultrathin nanosheet arrays: excellent energy storage, catalysis, photoconduction, and field-emitting performances. *J Phys Chem C* 116: 9319–9326.
182. Du Y, Yin Z, Rui X, et al. (2013) A facile, relative green, and inexpensive synthetic approach toward large-scale production of SnS_2 nanoplates for high-performance lithium-ion batteries. *Nanoscale* 5: 1456–1459.
183. He M, Yuan LX, Huang YH (2013) Acetylene black incorporated three-dimensional porous SnS_2 nanoflowers with high performance for lithium storage. *RSC Adv* 3: 3374–3383.
184. Li J, Wu P, Lou F, et al. (2013) Mesoporous carbon anchored with SnS_2 nanosheets as an advanced anode for lithium-ion batteries. *Electrochim Acta* 111: 862–868.
185. Sun H, Ahmad M, Luo J, et al. (2014) SnS_2 nanoflakes decorated multiwalled carbon nanotubes as high performance anode materials for lithium-ion batteries. *Mater Res Bull* 49: 319–324.
186. Balogun MS, Qiu W, Jian J, et al. (2015) Vanadium nitride nanowire supported SnS_2 nanosheets with high Reversible capacity as anode material for lithium ion batteries. *ACS Appl Mater Inter* 7: 23205–23215.
187. Wang Q, Huang Y, Miao J, et al. (2013) Graphene-supported Ce-SnS_2 nanocomposite as anode material for lithium-ion batteries. *J Am Ceram Soc* 96: 2190–2196.
188. Chen P, Su Y, Liu H, et al. (2013) Interconnected tin disulfide nanosheets grown on graphene

for Li-ion storage and photocatalytic applications. *ACS Appl Mater Inter* 5: 12073–12082.
189. Chang K, Wang Z, Huang G, et al. (2012) Few-layer SnS_2/graphene hybrid with exceptional electrochemical performance as lithium-ion battery anode. *J Power Sources* 201: 259–266.
190. Zhuo L, Wu Y, Wang L, et al. (2012) One-step hydrothermal synthesis of SnS_2/graphene composites as anode material for highly efficient rechargeable lithium ion batteries. *RSC Adv* 2: 5084–5087.
191. Yin J, Cao H, Zhou Z, et al. (2012) SnS_2@reduced graphene oxide nanocomposites as anode materials with high capacity for rechargeable lithium ion batteries. *J Mater Chem* 22: 23963–23970.
192. Wang Q, Nie YX, He B, et al. (2014) SnS_2/graphene nanocomposites as anodes of lithium-ion batteries. *Solid State Sci* 31: 81–84.
193. Liu S, Lu X, Xie J, et al. (2013) Preferential c-axis orientation of ultrathin SnS_2 nanoplates on graphene as high-performance anode for Li-ion batteries. *ACS Appl Mater Inter* 5: 1588–1595.
194. Zhang Q, Li R, Zhang M, et al. (2014) SnS_2/reduced graphene oxide nanocomposites with superior lithium storage performance. *Electrochim Acta* 115: 425–433.
195. Mei L, Xu C, Yang T, et al. (2013) Superior electrochemical performance of ultra-small SnS_2 nanocrystals decorated on flexible RGO in lithium-ion batteries. *J Mater Chem A* 1: 8658–8664.
196. Luo B, Fang Y, Wang B, et al. (2012) Two dimensional grapheme-SnS_2 hybrids with superior rate capability for lithium ion storage. *Energy Environ Sci* 5: 5226–5230.
197. Qin J, He C, Zhao N, et al. (2014) Graphene networks anchored with Sn@graphene as lithium ion battery anode. *ACS Nano* 8: 1728–1738.
198. Jiang X, Yang X, Zhu Y, et al. (2013) In situ assembly of graphene sheets-supported SnS_2 nanoplates into 3D macroporous aerogels for high-performance lithium ion batteries. *J Power Sources* 237: 178–186.
199. Zhao Y, Li X, Yan B, et al. (2015) Significant impact of 2D graphene nanosheets on large volume change tin-based anodes in lithium-ion batteries: A review. *J Power Sources* 274: 869–884.
200. Lei WX, Pan Y, Zhou YC, et al. (2014) CNTs-Cu composite layer enhanced Sn-Cu alloy as high performance anode materials for lithium-ion batteries. *RSC Adv* 4: 3233–3237.
201. Chen SY, Wang ZX, Fang XP, et al. (2011) characterization of TiS_2 as an anode material for lithium ion batteries. *Acta Phys Chim Sin* 27: 97–102.
202. Kartick B, Srivastava SK, Mahanty S (2013) TiS_2-MWCNT hybrid as highperformance anode in lithium-ion battery. *J Nanopart Res* 15: 1950–1962.
203. Deng D (2015) Li-ion batteries: basics, progress, and challenges. *Energy Sci Eng* 3: 385–418.
204. Rui X, Tan H, Yan Q (2014) Nanostructured metal sulfides for energy storage. *Nanoscale* 6: 9889–9924.
205. Son MY, Choi JH, Kang YC (2014) Electrochemical properties of bare nickel sulfide and nickel sulfide-carbon composites prepared by one-pot spray pyrolysis as anode materials for lithium secondary batteries. *J Power Sources* 251: 480–487.
206. Aso K, Sakuda A, Hayashi A, et al. (2013) All-solid-state lithium secondary batteries using NiS-carbon fiber composite electrodes coated with Li_2S-P_2S_5 solid electrolytes by pulsed laser deposition. *ACS Appl Mater Inter* 5: 686–690.

207. Aso K, Hayashi A, Tatsusago M (2012) Synthesis of NiS-carbon fiber composites in high-boiling solvent to improve electrochemical performance in all-solid-state lithium secondary batteries. *Electrochim Acta* 83: 448–453.
208. Sebastian ST, Jagan RS, Rajagoplan R, et al. (2014) Lithium-ion storage performance of camphoric carbon wrapped NiS nano/micro-hybrids *RSC Adv* 4: 11673–11679.
209. Geng H, Kong SF, Wang Y (2014) NiS nanorod-assembled nanoflowers grown on graphene: morphology evolution and Li-ion storage applications. *J Mater Chem A* 2: 15152–15158.
210. Pan Q, Xie J, Liu S, et al. (2013) Facile one-pot synthesis of ultrathin NiS nanosheets anchored on graphene and the improved electrochemical Li-storage properties. *RSC Adv* 3: 3899–3906.
211. Zhou W, Zheng JL, Yue YH, et al. (2015) Highly stable rGO-wrapped Ni_3S_2 nanobowls: Structure fabrication and superior long-life electrochemical performance in LIBs. *Nano Energy* 11: 428−435.
212. Gao Z, Song N, Zhang Y, et al. (2015) Cotton-textile-enabled, flexible lithium-ion batteries with enhanced capacity and extended lifespan. *Nano Lett* 15: 8194−8203.
213. Chen Q, Chen W, Ye JB, et al. (2015) L-Cysteine-assisted hydrothermal synthesis of nickel disulfide/graphene composite with enhanced electrochemical performance for reversible lithium storage. *J Power Sources* 294: 51–58.
214. Mahmoud N, Zhang C, Hou Y (2013) Nickel sulfide/nitrogen-doped graphene composites: phase-controlled synthesis and high performance a increased the grafting of node materials for lithium ion batteries. *Small* 9: 1321–1328.
215. Reddy ALM, Srivastava A, Gowda SR, et al. (2010) Synthesis of nitrogen-doped graphene films for lithium battery application. *ACS Nano* 4: 6337–6342.
216. Zhou Y, Yan D, Xu H, et al. (2015) Hollow nanospheres of mesoporous Co_9S_8 as a high-capacity and long-life anode for advanced lithium ion batteries. *Nano Energy* 12: 528−537.
217. Shi W, Zhu J, Rui X, et al. (2012) Controlled synthesis of carbon-coated cobalt sulfide nanostructures in oil phase with Enhanced Li Storage Performances. *ACS Appl Mater Inter* 4: 2999−3006.
218. Gu Y, Wang Y (2013) Graphene-Wrapped CoS Nanoparticles for high-capacity lithium-ion storage. *ACS Appl Mater Inter* 5: 801–806.
219. Zhang D, Mai YJ, Xiang JY, et al. (2012) FeS_2/C composite as an anode for lithium ion batteries with enhanced reversible capacity. *J Power Sources* 217: 229–235.
220. Gan Y, Xu F, Luo J, et al. (2016) One-pot biotemplate synthesis of FeS decorated sulfur-doped carbon fiber as high capacity anode for lithium-ion batteries. *Electrochim Acta* 209: 201–209.
221. Wen X, Wei X, Yang L, et al. (2015) Self-assembled FeS_2 cubes anchored on reduced graphene oxide as an anode material for lithium ion batteries. *J Mater Chem A* 3: 2090–2096.
222. Zhang SS, Tran DT (2015) Electrochemical verification of the redox mechanism of FeS_2 in a rechargeable lithium battery. *Electrochim Acta* 176: 784–789.
223. Cao F, Pan GX, Chen J, et al. (2016) Synthesis of pyrite/carbon shells on cobalt nanowires forming core/branch arrays as high-performance cathode for lithium ion batteries. *J Power Sources* 303: 35–40.
224. Cui H, Zhu G, Liu X, et al. (2015) Niobium nitride Nb_4N_5 as a new high-performance electrode material for supercapacitors. *Adv Sci* 2: 1500126.

225. Fu ZW, Wang Y, Yue XL, et al. (2004) Electrochemical reactions of lithium with transition metal nitride electrodes. *J Phys Chem B* 108: 2236–2244.
226. Balogun MS, Qiu W, Wang W, et al. (2015) Recent advances in metal nitrides as high-performance electrode materials for energy storage devices. *J Mater Chem A* 3: 1364–1387.
227. Miller TS, Jorge AB, Sella A, et al. (2015) The use of graphitic carbon nitride based composite anodes for lithium-ion battery applications. *Electroanal* 27: 2614–2619.
228. Tan G, Wu F, Yuan Y, et al. (2016) Free standing three-dimensional core-shell nanoarrays for lithium-ion battery anodes. *Nature Commun* 7: 11774.
229. Wang Y, Ding X, Huang L, et al. (2015) Critical influence of carbon nitride self-assembly coating on the electrochemical performance of SnO_2-TiO_2 nanocomposite anode material for lithium ion battery. *Int J Electrochem Sci* 11: 2461–2472.
230. Ulvestad A, Maehlen JP, Kirkengen M (2015) Silicon nitride coated silicon thin films as anodes for Li-ion batteries. *ECS Trans* 64: 107–111.
231. Wang R, Lang J, Zghang P, et al. (2015) Fast and large lithium storage in 3D porous VN nanowires-graphene composite as a superior anode toward high-performance hybrid supercapacitors. *Adv Func Mater* 25: 2270–2278.
232. Zhang K, Wang H, He X, et al. (2011) A hybrid material of vanadium nitride and nitrogen-doped graphene for lithium storage. *J Mater Chem* 21: 11916–11922.
233. Lei D, Yang T, Qu B, et al. (2014) Synthesis of TiN@C nanocomposites for enhanced electrochemical properties. *Sustain Ener* 2: 1–4.
234. Zheng H, Fang S, Tong Z, et al. (2015) Stabilized titanium nitride nanowire supported silicon core-shell nanorods as high capacity lithium-ion anodes. *J Mater Chem A* 3: 12476–12481.
235. Zhang J, Zhang J, Cai W, et al. (2012) Improving electrochemical properties of spinel lithium titanate by incorporation of titanium nitride via high-energy ball-milling. *J Power Sources* 211: 133–139.
236. Yue Y, Han P, He X, et al. (2012) In situ synthesis of a graphene/titanium nitride hybrid material with highly improved performance for lithium storage. *J Mater Chem* 22: 4938–4943.
237. Liu M, Zhang L, Han P, et al. (2015) Controllable formation of niobium nitride/nitrogen-doped graphene nanocomposites as anode materials for lithium-ion capacitors. *Part Part Syst Charact* 32: 1006–1011.
238. Li Y, Yan Y, Ming H, et al. (2014) One-step synthesis Fe_3N surface-modified Fe_3O_4 nanoparticles with excellent lithium storage ability. *Appl Surf Sci* 305: 683–688.
239. Liu J, Tang S, Lu Y, et al. (2013) Synthesis of MoN nanolayer coated MoO_2 hollow nanostructures as high-performance anode materials for lithium-ion batteries. *Energy Environ Sci* 6: 2691–2697.
240. Sun Q, Fu ZW (2012) Mn_3N_2 as a novel negative electrode material for rechargeable lithium batteries. *Appl Surf Sci* 258: 3197–3201.
241. Wu Y, Liu M, Feng H, et al. (2014) Carbon coated MnO@Mn_3N_2 core-shell composites for high performance lithium ion battery anodes. *Nanoscale* 6: 14697–14701.
242. Zhang L, Hu P, Zhao X, et al. (2011) Controllable synthesis of core-shell Co-CoO nanocomposites with a superior performance as an anode material for lithium-ion batteries. *J Mater Chem* 21: 18279–18283.

243. Xiong S, Chen JS, Lou XW, et al. (2012) Mesoporous Co_3O_4 and CoO-C topotactically transformed from chrysanthemum-like $Co(CO_3)_{0.5}(OH)\cdot 0.11H_2O$ and their lithium-storage properties. *Adv Funct Mater* 22: 861–871.
244. Qi Y, Du N, Zhang H, et al. (2012) CoO/NiSi*x* core-shell nanowire arrays as lithium-ion anodes with high rate capabilities. *Nanoscale* 4: 991–996.
245. Qi Y, Du N, Zhang H, et al. (2012) Nanostructured hybrid cobalt oxide/copper electrodes of lithium-ion batteries with reversible high-rate capabilities. *J Alloy Compd* 521: 83–89.
246. Zhao W, Du N, Zhang H, et al. (2016) A novel Co-Li_2O@Si core-shell nanowire array composite as a high-performance lithium-ion battery anode material. *Nanoscale* 8: 4511-4519.
247. Nethravathi C, Rajamathi CR, Rajamathi M, et al. (2013) N-doped graphene-VO_2(B) nanosheet-built 3D flower hybrid for lithium ion battery. *ACS Appl Mater Inter* 5: 2708–2714.
248. Zhang L, Wang Z, Yang K, et al. (2016) Preparation and electrochemical performances of CoO/3D graphene composite as anode for lithium-ion batteries. *J Alloy Compd* 656: 278–283.
249. Qi Y, Zhang H, Du N, et al. (2013) Highly loaded CoO/graphene nanocomposites as lithium-ion anodes with superior reversible capacity. *J Mat Chem A* 1: 2337–2342.
250. Zhu J, Zhu T, Zhou X, et al. (2011) Facile synthesis of metal oxide/reduced graphene oxide hybrids with high lithium storage capacity and stable cyclability. *Nanoscale* 3: 1084–1089.
251. Peng C, Chen B, Qin Y, et al. (2012) Facile ultrasonic synthesis of CoO quantum dot/graphene nanosheet composites with high lithium storage capacity. *ACS Nano* 6: 1074–1081.
252. Sun Y, Hu X, Luo W, et al. (2012) Ultrathin CoO/graphene hybrid nanosheets: a highly stable anode material for lithium-ion batteries. *J Phys Chem C* 116: 20794–20799.
253. Verrelli R, Hassoun J (2015) High-capacity NiO-(mesocarbon microbeads) conversion anode for lithium-ion battery. *ChemElectroChem* 2: 988–994.
254. Sun X, Yan C, Chen Y, et al. (2014) Three-dimensionally curved NiO nanomembranes as ultrahigh rate capability anodes for Li-ion batteries with long cycle lifetimes. *Adv Energy Mater* 4.
255. Chen X, Zhang N, Sun K (2012) Facile ammonia-induced fabrication of nanoporous NiO films with enhanced lithium-storage properties. *Electrochem Commun* 20: 137–140.
256. Huang XH, Yuan YF, Wang Z, et al. (2011) Electrochemical properties of NiO/Co-P nanocomposite as anode materials for lithium ion batteries. *J Alloy Compd* 509: 3425–3429.
257. Zou Y, Wang Y (2011) NiO nanosheets grown on graphene nanosheets as superior anode materials for Li-ion batteries. *Nanoscale* 3: 2615–2620.
258. Huang Y, Huang XL, Lian JS, et al. (2012) Self-assembly of ultrathin porous NiO nanosheets/graphene hierarchical structure for high-capacity and high-rate lithium storage. *J Mater Chem* 22: 2844–2847.
259. Zhu XJ, Hu J, Dai HL, et al. (2012) Reduced graphene oxide and nanosheet-based nickel oxide microsphere composite as an anode material for lithium ion battery. *Electrochim Acta* 64: 23–28.
260. Choi SH, Ko YN, Lee JK, et al. (2014) Rapid continuous synthesis of spherical reduced graphene ball-nickel oxide composite for lithium ion batteries. *Sci Rep* 4: 5786.
261. Zhou F, Chen Y, Liu K, et al. (2016) Metal organic frameworks derived hierarchical hollow NiO/Ni/graphene composites for lithium and sodium storage. *ACS Nano* 10: 377−386.

262. Zhong KF, Xia X, Zhang B, et al. (2010) MnO powder as anode active materials for lithium ion batteries. *J Power Sources* 195: 3300–3308.
263. Li SR, Sun Y, Ge SY, et al. (2012) A facile route to synthesize nano-MnO/C composites and their application in lithium ion batteries. *Chem Eng J* 192: 226–231.
264. Zhong K, Zhang B, Luo S, et al. (2011) Investigation on porous MnO microsphere anode for lithium ion batteries. *J Power Sources* 196: 6802–6808.
265. Tang X, Sui G, Cai Q, et al. (2016) Novel MnO/carbon composite anode material with multi-modal pore structure for high performance lithium-ion batteries. *J Mater Chem A* 4: 2082–2088.
266. Xia Y, Xiao Z, Dou X, et al. (2013) Green and facile fabrication of hollow porous MnO/C microspheres from microalgaes for lithium-ion batteries. *ACS Nano* 7: 7083–7092.
267. Yue J, Gu X, Wang N, et al. (2014) General synthesis of hollow MnO_2, Mn_3O_4 and MnO nanospheres as superior anode materials for lithium ion batteries. *J Mater Chem A* 2: 17421–17426.
268. Liu B, Hu X, Xu H, et al. (2014) Encapsulation of MnO nanocrystals in electrospun carbon nanofibers as high-performance anode materials for lithium-ion batteries. *Sci Rep* 4: 4229.
269. Sun Y, Hu X, Luo W, et al. (2013) Reconstruction of conformal nanoscale MnO on graphene as a high-capacity and long-life anode material for lithium ion batteries. *Adv Func Mater* 23: 2436–2443.
270. Jiang H, Hu YJ, Guo SJ, et al. (2014) Rational design of MnO/carbon nanopeapods with internal void space for high-rate and long-life Li-ion batteries. *ACS Nano* 8: 6038–6046.
271. Wang Y, Han ZJ, Yu SF, et al. (2013) Core-leaf onion-like carbon/MnO_2 hybrid nano-urchins for rechargeable lithium-ion batteries. *Carbon* 64: 230–236.
272. Lai H, Li JX, Chen ZG, et al. (2012). Carbon nanohorns as a high-performance carrier for MnO_2 anode in lithium-ion batteries. *ACS Appl Mater Inter* 4: 2325–2328.
273. Xia H, Lai M, Lu L (2010) Nanoflaky MnO_2/carbon nanotube nanocomposites as anode materials for lithium-ion batteries. *J Mater Chem* 20: 6896–6902.
274. Yun YS, Kim JM, Park HH, et al. (2013) Free-standing heterogeneous hybrid papers based on mesoporous γ-MnO_2 particles and carbon nanotubes for lithium-ion battery anodes. *J Power Sources* 244: 747–751.
275. Yu AP, Park HW, Davies A, et al. (2011) Free-standing layer-by-layer hybrid thin film of graphene-MnO_2 nanotube as anode for lithium ion batteries. *J Phys Chem Lett* 2: 1855–1860.
276. Li L, Raji ARO, Tour JM (2013) Graphene-wrapped MnO_2-graphene nanoribbons as anode materials for high-performance lithium ion batteries. *Adv Mater* 25: 6298–6302.
277. Li YY, Zhang QW, Zhu JL, et al. (2014) An extremely stable MnO_2 anode incorporated with 3D porous graphene-like networks for lithium-ion batteries. *J Mater Chem A* 2: 3163–3168.
278. Luo W, Hu X, Sun Y, et al. (2011) Electrospinning of carbon-coated Mo_2 nanofibers with enhanced lithium-storage properties. *Phys Chem Chem Phys* 13: 16735–16740.
279. Liu B, Zhao X, Tian Y, et al. (2013) A simple reduction process to synthesize MoO_2/C composites with cage-like structure for high-performance lithium-ion batteries. *Phys Chem Chem Phys* 15: 8831–8837.
280. Gao Q, Yang L, Lu X, et al. (2010) Synthesis, characterization and lithium-storage performance

of MoO_2/carbon hybrid nanowires. *J Mater Chem* 20: 2807–2812.
281. Zeng L, Zheng C, Deng C, et al. (2013) MoO_2-ordered mesoporous carbon nanocomposite as an anode material for lithium-ion batteries. *ACS Appl Mater Inter* 5: 2182–2187.
282. Ihsan M, Wang H, Majid SR, et al. (2016) MoO_2/Mo_2C/C spheres as anode materials for lithium ion batteries. *Carbon* 96: 1200–1207.
283. Xu Y, Yi R, Yuan B, et al. (2012) High capacity MoO_2/graphite oxide composite anode for lithium-ion batteries. *J Phys Chem Lett* 3: 309–314.
284. Sun Y, Hu X, Luo W, et al. (2011) Self-assembled hierarchical MoO_2/graphene nanoarchitectures and their application as a high-performance anode material for lithium-ion batteries. *ACS Nano* 5: 7100–7107.
285. Tang Q, Shan Z, Wang L, et al. (2012) MoO_2-graphene nanocomposite as anode material for lithium-ion batteries. *Electrochim Acta* 79: 148–153.
286. Hou Y, Li JY, Wen ZH, et al. (2014) N-doped graphene/porous g-C_3N_4 nanosheets supported layered-MoS_2 hybrid as robust anode materials for lithium-ion batteries. *Nano Energy* 8: 157–164.
287. Kumar V, Lee PS (2015) Redox active polyaniline-h-MoO_3 hollow nanorods for improved pseudocapacitive performance. *J Phys Chem C* 119: 9041–9049.
288. Brezesinski T, Wang J, Tolbert SH, et al. (2010) Ordered mesoporous α-MoO_3 with iso-oriented nanocrystalline walls for thin-film pseudocapacitors. *Nat Mater* 9: 146–151.
289. Zhou K, Zhou W, Liu X, et al. (2015) Ultrathin MoO_3 nanocrystals self-assembled on graphene nanosheets via oxygen bonding as supercapacitor electrodes of high capacitance and long cycle life. *Nano Energy* 12: 510–520.
290. Han B, Lee KH, Lee YW, et al. (2015) MoO_3 nanostructured electrodes prepared via hydrothermal process for lithium ion batteries. *Int J Electrochem Sci* 10: 4232–4240.
291. Wang Q, Sun J, Wang Q, et al. (2015) Electrochemical performance of α-MoO_3-In_2O_3 core-shell nanorods as anode materials for lithium-ion batteries. *J Mater Chem A* 3: 5083–5091.
292. Hamed B, Shahid M, Nagae-raju DH, et al. (2015) Surface passivation of MoO_3 nanorods by atomic layer deposition toward high rate durable Li ion battery anodes. *ACS Appl Mater Inter* 7: 13154–13163.
293. Zhao G, Li C, Zhang L, et al. (2015) "Sea cucumber"-like Ti@MoO_3 nanorod arrays as self-supported lithium ion battery anodes with enhanced rate capability and durability. *J Mater Chem A* 3: 22547–22551.
294. Ma F, Yuan A, Xu J, et al. (2015) Porous α-MoO_3/MWCNT nanocomposite synthesized via a surfactant-assisted solvothermal route as a lithium-ion-battery high-capacity anode material with excellent rate capability and cyclability. *ACS Appl Mater Inter* 7: 15531–15541.
295. Tauseef A, Li W, Li J, et al. (2016) Lithium storage study on MoO_3-grafted TiO_2 nanotube arrays. *Appl Nanoscience* [in press].
296. Xue XY, Chen ZH, Xing LL, et al. (2011) SnO_2/MoO_3 core-shell nanobelts and their extraordinarily high reversible capacity as lithium-ion battery anodes. *Chem Commun* 47: 5205–5207.
297. Hashem AM, Abbas SB, Abdel-Ghany AE, et al. (2016) Blend formed by oxygen deficient $MoO_{3-\delta}$ oxides as lithium-insertion compounds. *J Alloy Compd* 686: 744–752.

298. Bruck A, Cama CA, Gannett CN, et al. (2016) Nanocrystalline iron oxide based electroactive materials in lithium ion batteries: the critical role of crystallite size, morphology, and electrode heterostructure on battery relevant electrochemistry. *Inorg Chem Front* 3: 26–40.
299. Zhang WM, Wu XL, Hu JS, et al. (2008) Carbon-coated Fe_3O_4 nanospindles as a superior anode material for lithium-ion batteries. *Adv Funct Mater* 18: 3941–3946.
300. Zhu T, Chen JS, Lou XW (2011) Glucose-assisted one-pot synthesis of FeOOH nanorods and their transformation to Fe_3O_4@carbon nanorods for application in lithium ion batteries. *J Phys Chem C* 115: 9814–9820.
301. Chen JS, Zhang YM, Lou XW (2011) One-pot synthesis of uniform Fe_3O_4 nanospheres. *ACS Appl Mater Inter* 3: 3276–3279.
302. Wang ZY, Luan DY, Madhavi S, et al. (2012) Assembling carbon-coated γ-Fe_2O_3 hollow nanohorns on the CNT backbone for superior lithium storage capability. *Energ Environ Sci* 5: 5252–5256.
303. Ji L, Toprakci O, Alcoutlabi M, et al. (2012) α-Fe_2O_3 nanoparticle-loaded carbon nanofibers as stable and high-capacity anodes for rechargeable lithium-ion batteries. *ACS Appl Mater Inter* 4: 2672–2679.
304. Sun Z, Madej E, Genç A, et al. (2016) Demonstrating the steady performance of iron oxide composites over 2000 cycles at fast charge-rates for Li-ion batteries. *Chem Commun* 52: 7348–7351.
305. Jang B, Park M, Chae OB, et al. (2012) Direct synthesis of self-assembled ferrite/carbon hybrid nanosheets for high performance lithium-ion battery anodes. *J Am Chem Soc* 134: 15010–15015.
306. He CN, Wu S, Zhao NQ, et al. (2013) Carbon-encapsulated Fe_3O_4 nanoparticles as a high-rate lithium-ion battery anode material. *ACS Nano* 7: 4459–4469.
307. Zhu X, Zhu Y, Murali S, et al. (2011) Nanostructured reduced graphene oxide/Fe_2O_3 composite as a high-performance anode material for lithium ion batteries. *ACS Nano* 5: 3333–3338.
308. Wang G, Liu T, Luo Y, et al. (2011) Preparation of Fe_2O_3/graphene composite and its electrochemical performance as an anode material for lithium ion batteries. *J Alloy Compd* 509: L216–L220.
309. Shi M, Wu T, Song X, et al. (2016) Active Fe_2O_3 nanoparticles encapsulated in porous g-C_3N_4/graphene sandwich-type nanosheets as superior anode for high-performance lithium-ion batteries. *J Mater Chem A* [in press].
310. Wang R, Xu C, Sun J, et al. (2013) Flexible free-standing hollow Fe_3O_4/graphene hybrid films for lithium-ion batteries. *J Mater Chem A* 1: 1794–1800.
311. Zhuo L, Wu Y, Wang L, et al. (2013) CO_2-expanded ethanol chemical synthesis of a Fe_3O_4/graphene composite and its good electrochemical properties as anode material for lithium-ion batteries. *J Mater Chem A* 1: 3954–3960.
312. Pan L, Zhu XD, Xie XM, et al. (2015) Smart hybridization of anatase TiO_2 nanorods and Fe_3O_4 nanoparticles with pristine graphene nanosheets: hierarchically nanoengineered ternary heterostructures for high-rate lithium storage. *Adv Func Mater* 25: 3341–3350.
313. Mo R, Lei Z, Sun K, et al. (2014) Facile synthesis of anatase TiO_2 quantum-dot/graphene-nanosheet composites with enhanced electrochemical performance for

lithium-ion batteries. *Adv Mater* 26: 2084–2088.
314. Ding S, Chen JS, Luan D, et al. (2011) Graphene-supported anatase TiO_2 nanosheets for fast lithium storage. *Chem Commun* 47: 5780–5782.
315. Qiu B, Xing M, Zhang J (2014) Mesoporous TiO_2 nanocrystals grown in situ on graphene aerogels for high photocatalysis and lithium-ion batteries. *J Am Chem Soc* 136: 5852–5855.
316. Li W, Wang F, Feng S, et al. (2013) Sol-gel design strategy for ultradispersed TiO_2 nanoparticles on graphene for high-performance lithium ion batteries. *J Am Chem Soc* 135: 18300–18303.
317. Gao L, Hu H, Li G, et al. (2014) Hierarchical 3D TiO_2@Fe_2O_3 nano-framework arrays as high-performance anode materials. *Nanoscale* 6: 6463–6467.
318. Yan C, Chen G, Sun J, et al. (2016) Novel anode of C&N co-doped Co_3O_4 hollow nanofibres with excellent performance for lithium-ion batteries. *Phys Chem Chem Phys* [in press].
319. Yang H, Wang Y, Nie Y, et al. (2016) Co_3O_4/porous carbon nanofibers composite as anode for high-performance lithium ion batteries with improved cycle performance and lithium storage capacity. *J Compos Mate*r [in press].
320. Zhu X, Ning G, Ma X, et al. (2013) High density Co_3O_4 nanoparticles confined in a porous graphene nanomesh network driven by an electrochemical process: ultra-high capacity and rate performance for lithium ion batteries. *J Mater Chem A* 1: 14023–14030.
321. Li BJ, Cao HQ, Shao J, et al. (2011) Co_3O_4@graphene composites as anode materials for high-performance lithium ion batteries. *Inorg Chem* 50: 1628–1632.
322. Kim H, Seo DH, Kim SW, et al. (2011) Highly reversible Co_3O_4/graphene hybrid anode for lithium rechargeable batteries. *Carbon* 49: 326–332.
323. Sun H, Liu Y, Yu Y, et al. (2014) Mesoporous Co_3O_4 nanosheets-3D graphene networks hybrid materials for high-performance lithium ion batteries. *Electrochim Acta* 118: 1–9.
324. Li P, Cui M, Zhang M, et al. (2016) Facile fabrication of Co_3O_4/nitrogen-doped graphene hybrid materials as high performance anode materials for lithium ion batteries. *CrystEngComm* 18: 3383–3388.
325. Dou Y, Xu J, Ruan B, et al. (2016) Atomic layer-by-layer Co_3O_4/graphene composite for high performance lithium-ion batteries. *Adv Energy Mater* 6.
326. Wang HG, Ma DL, Huang Y, et al. (2012) General and controllable synthesis strategy of metal oxide/TiO_2 hierarchical heterostructures with improved lithium-ion battery performance. *Sci Rep* 2: 136–136.
327. Weng BC, Xu FH, Lozano K (2014) Mass production of carbon nanotube-reinforced polyacrylonitrile fine composite fibers. *J Appl Polym Sci* 131: 2928–2935.

AIMS Press